Drug Metabolism Letters, 2018, *12*, 33-53

RESEARCH ARTICLE

In vitro Drug Metabolism Investigation of 7-Ethoxycoumarin in Human, Monkey, Dog and Rat Hepatocytes by High Resolution LC-MS/MS

Wan-Yong Feng*, Jenny Wen and Kathe Stauber

Drug Metabolism and Pharmacokinetics, Dart NeuroScience, San Diego, CA 92131, USA

Abstract: ***Background*:** Recently, it has been an increasing concern on the bioactivation and adverse reactions associated with consumption of herbal and nature products. 7-Ethoxycoumarin is one of coumarin family compounds, but little information is available regarding its potential reactive metabolites.

***Method*:** 7-ethoxylcoumarin was incubated individually with human, monkey, dog and rat hepatocytes for 2 hr, metabolites were detected, identified and characterized using high resolution liquid chromagraphy – tandem mass spectrometry.

***Results*:** Twenty-eight metabolites (M1 - M28) were detected and identified. O-deethylation, glucuronidation, sulfation, oxygenation, oxidative ring-opening, hydrogenation, glutathionation, dehydrogenation, cysteination, glucosidation, methylation, and hydrolysis were observed. At least sixteen metabolites not reported previously, were newly identified. M1 (O-deethylation, mono-oxygenation and glucuronidation), M3 (O-deethylation and glucuronidation), M5 (hydrolysis and mono-oxygenation), M14 (O-deethylation), M16 (hydrolysis), M22 (oxidative ring-opening and oxygenation) and M27 (mono-oxygenation) exhibited high mass spectrometric responses in human hepatocytes. M3, M5, M8, M13 (mono-oxygenation), M14, M16, M18 (O-deethylation and sulfation), M22 and M27 exhibited high mass spectrometric responses in monkey hepatocytes. M14, M16, M18, M20 (glutathionation and dehydrogenation) and M27 exhibited high mass spectrometric responses in dog hepatocytes. M1 (O-deethylation, mono-oxygenation and glucuronidation), M3, M5, M13, M14, M16, M17 (cysteination), M18, M20, and M22 exhibited high mass spectrometric responses in rat hepatocytes.

***Conclusion*:** Most of new metabolites *via* oxidative ring-opening and glutathionation were identified. Species differences in metabolism of 7-ethoxylcoumarin in hepatocytes were observed. The analysis of metabolites suggests that 7-ethoxylcoumarin may undergo 3,4-epoxidation responsible for formation of glutathione and its derived cysteine conjugates, carboxylic acid and its glucuronides, glucosides and sulfate.

ARTICLE HISTORY

Received: January 01, 2018
Revised: March 18, 2018
Accepted: April 12, 2018

DOI:
10.2174/1872312812666180418142056

Keywords: 7-ethoxycoumarin, metabolism, humans, monkeys, dogs, rats, hepatocytes.

1. INTRODUCTION

In the recent years, it has become an increasing concern on the bioactivation and adverse reactions associated with consumption of herbal and nature products. Coumarin is a natural product widely used in foodstuffs and cosmetic products. The studies have showed that coumarin exhibited remarkable species differences in both metabolism and toxicity [1-3]. The marked difference in metabolism of coumarin was found between rodent species (rats and mice) and other species including humans. 7-hydroxylation pathway of coumarin that is a major pathway in humans but only a minor pathway in rats and mice, is considered as a detoxification pathway. In contrast, the major metabolic route of coumarin in rats and mice is a 3,4-epoxidation pathway resulting in the formation of toxic 2-hydroxyphenylacetaldehyde. 7-hydroxycoumarin known as umbelliferone is a naturally occurring coumarin derivative and a dominant metabolite of 7-ethoxycoumarin. 7-Ethoxycoumarin is a synthetic coumarin derivative. Both 7-hydroxycoumarin and 7-ethoxycoumarin are also cosmetic ingredients [4], but their bioactivation information is still unknown. On the other hand, coumarin and its family members have recently drawn much attention due to their broad pharmacological activities such as antimicrobial, anti-tumor, anti-viral, anti-inflammatory and antioxidant properties [5, 6]. The metabolic liability of the key structural core within a coumarin family is crucial for the design and development of new analogues. Metabolism of 7-ethoxycoumarin in human liver microsomes was studied as early as in 1985 [7-10]. Its primary metabolic pathways have been reported as O-deethylation and subsequential glucuron-

*Address correspondence to this author at the Drug Metabolism and Pharmacokinetics, Dart NeuroScience, 12278 Scripps Summit Drive, San Diego, California 92131, USA; Tel: 858.736.0252; Fax: 858.246.8217; E-mails: wyfeng2k@yahoo.com, wfeng@dartneuroscience.com

idation and sulfation in *in vitro* human [11-13], monkey [12, 14], dog [15], rat [12, 16-23], pig [12, 15, 24], mouse [12, 18], rabbit [25], hen [26], trout [27] and bacterial systems [28-32]. Metabolites and Metabolic pathways of 7-ethoxycoumarin in humans, monkeys, dogs and rats reported in the literatures, are summarized in Scheme **1**. Ultilizing its primary metabolic pathways, 7-ethoxycoumarin is one of the most commonly used probe substances for metabolic stability, and CYP1A2, 2A6, 2B6, 2D6, 2E1, and 2C9 O-deethylation activity assessment [7-10]. Although O-deethylation and subsequential glucuronidation and sulfation of 7-ethoxycoumarin have been routinely observed in *in vitro* animal and human systems, bioactivation and species difference of 7-ethoxycoumarin has not been reported yet. Since the properties of pharmacokinetics and absorption, distribution, metabolism, excretion of coumarin family members are essential for determining their potential bioactivities, the mechanism of *in vivo* efficacy, and toxicity, it is of great interest and importance to understand comprehensive biotransformation of 7-ethoxycoumarin across different species. In this study, metabolism of 7-ethoxycoumarin in human, monkey, dog, and rat hepatocytes was studied. Metabolites were searched and identified, and metabolic profiles were determined and compared across these species.

2. MATERIALS AND METHODS

2.1. Materials and Reagents

7-Ethoxycoumarin (purity: 99.5%), and other reagents such as acetonitrile and formic acid were purchased from Sigma-Aldrich (St. Louis, MO). Cryopreserved human, Cynomolgus monkey, Beagle dog and Sprague Dawley (SD) rat hepatocytes pooled from 10 donors of males and females, 3 males, 3 males and 30 males, respectively, were purchased from Bioreclamation-IVT (Baltimore, Maryland). Hepatocytes thawing (*InVitro*GRO HT) and incubation (Krebs-Henseleit Buffer, KHB) media were also purchased from Bioreclamation-IVT. 24-well BD Falcon plates were purchased from Corning (Coning, NY).

2.2. *In-vitro* Incubations

Cryopreserved hepatocyte vials containing human, Cynomolgus monkey, Beagle dog, and SD rat hepatocytes were removed from the liquid nitrogen storage tank and quickly placed in a water bath at 37 °C for about 2 minutes. Contents of the cryopreservation vials were gently poured into 48 mL of pre-warmed *InVitro*GRO HT medium and rinsed twice, each with 1.0 mL of the medium. The cell suspension was mixed by gentle inversion and centrifuged at approximately 50 × g (Beckman Coulter, Brea, CA) for 5 min at room temperature. The cell pellets were gently re-suspended with 2 - 3 mL KHB medium. The viabilities of hepatocytes were measured and ranged from 82% to 96%. The volume of cell suspension was adjusted with KHB medium to obtain a cell concentration of 2.0×10^6 cells/mL.

7-Ethoxycoumarin (10 μM) was incubated with 1.0×10^6 cells/mL of hepatocytes in KHB medium on a 24-well plate at 37 °C with 5% CO_2 and 95% humidity with gentle rotary shaking (80 rpm, MaxQ2000 shaker, Thermo Scientific, Waltham, MA) inside a water jacketed CO_2 incubator (Thermo Scientific, Asheville, NC) for 120 min. The total volume for each species was 1.2 mL. 0.6 mL reaction solution was taken at 0 min and mixed with 0.6 mL of ice-cold acetonitrile. The reaction at 120 min was quenched with 0.6 mL of ice-cold acetonitrile. The resulting solution was mixed well, and then centrifuged (Eppendorf, Hauppauge, NY) at 13,000 rpm for 5 min at 5 °C. The supernatant was transferred into a new tube and then dried with a FreeZone Freeze dryer (Labconco, Kansas City, MO) overnight. The residue was reconstituted with 0.6 mL of 10% acetonitrile/0.1% formic acid, and centrifuged again. The supernatants were transferred onto a 96-well plate and 20 μL sample was injected onto a LC-Q-Exactive Plus system for the analysis.

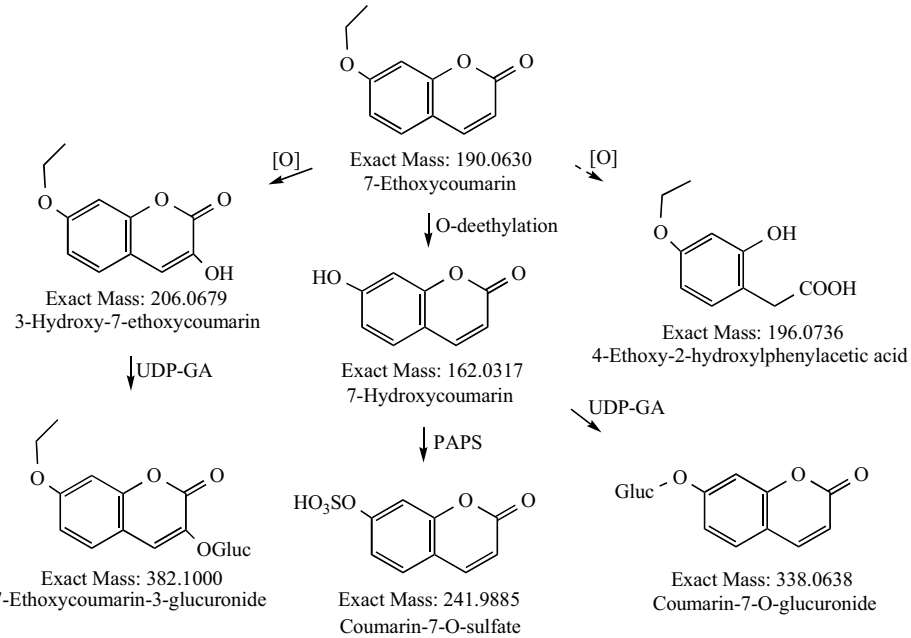

Scheme 1. A summary for observed metabolites and metabolic pathways of 7-exthoxycoumarin in humans, monkeys, dogs and rats reported in the literatures.

2.3. Bioanalytical Methods

The processed samples were analyzed on an UltiMate 3000 - Q-Exactive Plus system. Thermo Xcalibur was used for system control, data acquisition and processing. Q-Exactive Plus was operated in the positive (+) and negative ion (-) modes with an electrospray ionization source (HESI-II). The capillary temperature was set at 360 °C. The ionization voltage was set at 3.5 kV. Sheath gas and auxiliary gas flow were set as 35 and 13, respectively. S-lens RF level was 50 V. The mass resolution was set as 70,000 for full MS, and 17,500 for dd-MS2 scans. The collision energies were set at 45 ± 10 V, and 15 ± 10 V.

The HPLC system consisted of a Dionex UltiMate 3000 including degasser, binary quaternary gradient pumps, column heater, and an autosampler. 7-Ethoxycoumarin and its metabolites were separated on a 150 × 20 mm, 3 μm, Luna C18(2) column (Phenomenex, Torrance, CA). The mobile phase system consisted of solution A (0.1% formic acid in water) and solution B (0.1% formic acid in acetonitrile) at 0.32 mL/min with a 24-min gradient (0 - 0.5 min keeping at 8% B, 0.5 - 20.0 min from 8% to 48% B, 20.0 - 20.1 min from 48 to 95% B, 20.1 - 21.0 min keeping at 95% B, 21.0 - 21.1 min from 95 to 8% B, 21.1 - 24.0 min keeping at 8% B).

Metabolites were searched and confirmed further using the LC-MS/MS method. Collisionally induced dissociation (CID) or fragmentation spectra of 7-ethoxycoumarin and its individual metabolites were compared for further confirmation of individual metabolites. The structures of metabolites were elucidated by the comparative analysis of fragment ions between the parent and individual metabolites. ChemDraw Ultra 7.0 (PerkinElmer, Waltham, MA) was used to assist exact mass calculation and the chemical structure elucidation of predicted metabolites, and chemical structure elucidation of fragment ions obtained from MS/MS data acquisition. It should be pointed out that our primary purpose was to identify and characterize metabolites across four species (humans, monkeys, dogs and rats), and tentatively to rank metabolites based on their mass spectrometric responses in each species. Preliminary percent abundances of metabolites were estimated by assuming that 7-ethoxycourmarin and its metabolites had approximately same ionization efficiencies and their mass spectrometric responses over the concentration range were linear. When the mass spectrometric response peak areas of each metabolite were compared across four species, the ionization efficiency difference could be neglected. The percent abundances were calculated by selected ion chromatogram peak areas of 7-ethoxycoumarin and its metabolites in positive ion mode. Since 7-ethoxycoumarin and some of its metabolites were not ionized and detected in negative ion mode, the percent abundances of 7-ethoxycoumarin and its metabolites were not calculated but expressed in detected or not detected. In the following figure presentations of selected ion chromatograms, only 8 highest abundant peaks corresponding 8 *m/z* values were selected due to software limitation.

3. RESULTS AND DISCUSSION

3.1 Metabolite Profiles

Experimental results for 7-ethoxycoumarin in cryopreserved human, monkey, dog, and rat hepatocytes are summarized in Table **1**. O-deethylation, glucuronidation, sulfation, oxygenation, oxidative ring-opening, hydrogenation, glutathionation, dehydrogenation, cysteination, glucosidation, methylation, and hydrolysis were observed. Twenty-eight metabolites (M1 – M28) were detected, further confirmed and characterized using LC-MS^n (n = 1 – 2) in positive ion mode. All metabolites had a shorter retention time than the parent. Preliminary percent abundances of 7-ethoxycoumarin and its metabolites were estimated by their mass spectrometric response peak areas. The percent abundances of metabolites with ≥ 0.3% were considered as major metabolites. In negative ion mode, 7-ethoxycoumarin and its metabolites were only classified as detected or not detected. Highlighted values in Table **1** indicated that metabolites were also detected in negative ion mode. Figs. (**1-4)** show selected positive ion chromatograms of 7-ethoxycoumarin and its metabolites detected in human, monkey, dog, and rat hepatocytes, respectively. Figs. (**5-8**) show selected negative ion chromatograms of metabolites detected in human, monkey, dog, and rat hepatocytes, respectively.

Table 1. Summary for percent abundances of metabolites of 7-ethoxycoumarin generated in human, monkey, dog, and rat hepatocytes.

	RT (min)	*m/z (+)*	Biotransformation Pathway	Human	Monkey	Dog	Rat
M1	4.82	355.0660	O-deethylation, mono-oxygenation and glucuronidation	**0.4**	**0.2**	**0.0**	**0.3**
M2	5.18	325.0918	O-deethylation and glucosidation	ND	ND	ND	0.0
M3	5.43	339.0711	O-deethylation and glucuronidation	**2.0**	**15.3**	**0.1**	**11.6**
M4	6.83	179.0339	O-deethylation and mono-oxygenation	0.0	0.0	ND	0.0
M5	7.17	225.0757	Hydrolysis and mono-oxygenation	**2.5**	0.3	0.0	0.8
M6	7.78	383.0973	mono-oxygenation and glucuronidation	**0.0**	0.0	**0.2**	**0.0**
M7	8.12	179.0339	O-deethylation and mono-oxygenation	0.0	0.0	0.0	ND
M8	9.01	373.1129	Oxidative ring-opening, mono-oxygenation and glucosidation	**0.0**	**0.4**	ND	ND

(Table 1) Contd…

	RT (min)	*m/z (+)*	Biotransformation Pathway	Human	Monkey	Dog	Rat
M9	9.06	359.1336	Oxidative ring-opening, mono-oxygenation and glucuronidation	ND	ND	ND	**ND**
M10	9.27	359.1336	Oxidative ring-opening, mono-oxygenation and glucuronidation	**ND**	**ND**	**ND**	**ND**
M11	9.62	373.1129	Oxidative ring-opening, mono-oxygenation and glucosidation	**ND**	**ND**	ND	**ND**
M12	9.71	258.9907	O-deethylation, mono-oxygenation and sulfation	**ND**	**0.0**	**0.0**	**0.1**
M13	9.75	207.0652	Mono-oxygenation	0.1	0.4	0.0	0.3
M14	9.81	163.0390	O-deethylation (producing 7-HC)	1.1	20.3	1.2	19.7
M15	9.86	193.0495	O-deethylation and mono-oxygenation, methylation	ND	0.0	0.0	**0.1**
M16	10.23	209.0808	Hydrolysis	**0.3**	**0.5**	**0.3**	**0.3**
M17	10.61	310.0744	Glutathionation and dehydrogenation with glycine & glutamine hydrolysis	**0.2**	**0.0**	**0.0**	**1.1**
M18	10.87	242.9958	O-deethylation and sulfation	**0.2**	**4.3**	**0.4**	**4.6**
M19	10.96	181.0859	Oxidative ring-opening (producing RCH2CHO)	0.1	0.3	0.1	0.1
M20	11.49	496.1384	Glutathionation and dehydrogenation	**0.0**	**0.0**	**0.4**	**0.7**
M21	12.2	207.0652	Mono-oxygenation	0.0	0.0	0.0	0.1
M22	12.37	197.0808	Oxidative ring-opening and mono-oxygenation (producing RCH2COOH)	**1.8**	**1.5**	**0.2**	**1.2**
M23	12.4	183.1016	Oxidative ring-opening and hydrogenation (producing RCH2CH2OH)	**0.1**	**0.0**	**0.1**	**0.1**
M24	12.47	207.0652	Mono-oxygenation	0.1	0.1	0.0	0.1
M25	13.21	277.0376	Oxidative ring-opening, mono-oxygenation and sulfation	**ND**	**ND**	**ND**	**ND**
M26	15.43	310.0744	Glutathionation and dehydrogenation with glycine & glutamine hydrolysis	**0.0**	**0.0**	**ND**	**0.1**
M27	16.85	207.0652	Mono-oxygenation	**0.5**	**0.3**	**0.4**	**0.1**
M28	17.3	207.0652	Mono-oxygenation	0.0	0.0	0.0	0.1
P	18.81	191.0703		90.7	55.9	96.6	58.5

Note: a. P = Parent (7-ethoxycoumarin), M = Metabolite, *m/z* = monoisotopic mass to charge ratio in positive ion mode; b. ND = Not Detected in positive ion mode under these experimental conditions c. the values are less than 0.05% were considered as zero; d. highlighted values indicating detected metabolites in negative ion mode with less *m/z* value of 2.0146.

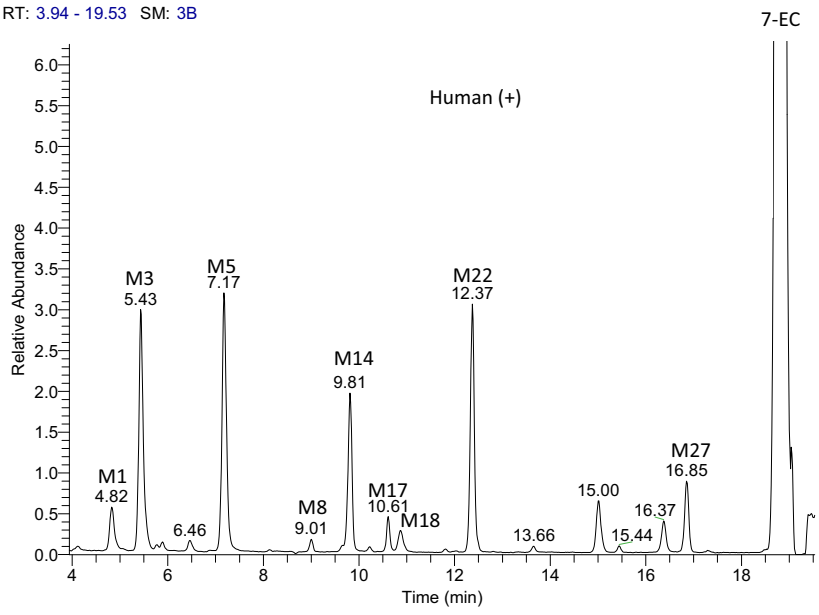

Fig. (1). Selected ion chromatograms of 7-ethoxycoumarin and its metabolites in human hepatocytes in positive ion mode (note: M16 was not selected).

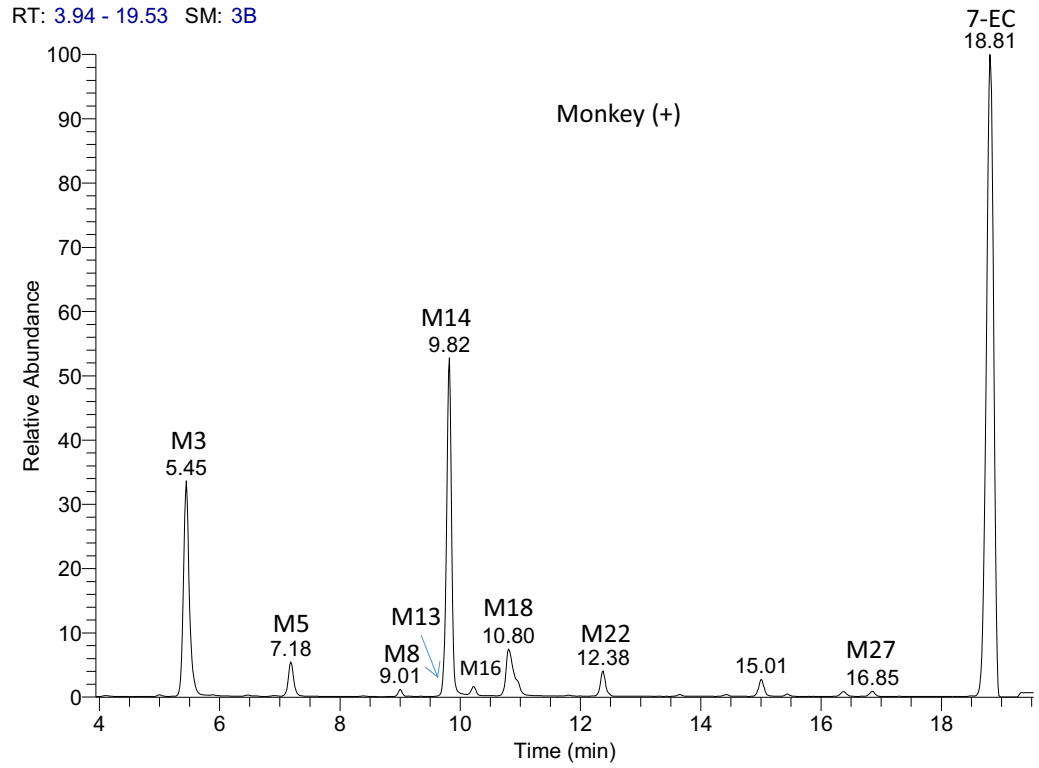

Fig. (2). Selected ion chromatograms of 7-ethoxycoumarin and its metabolites in monkey hepatocytes in positive ion mode.

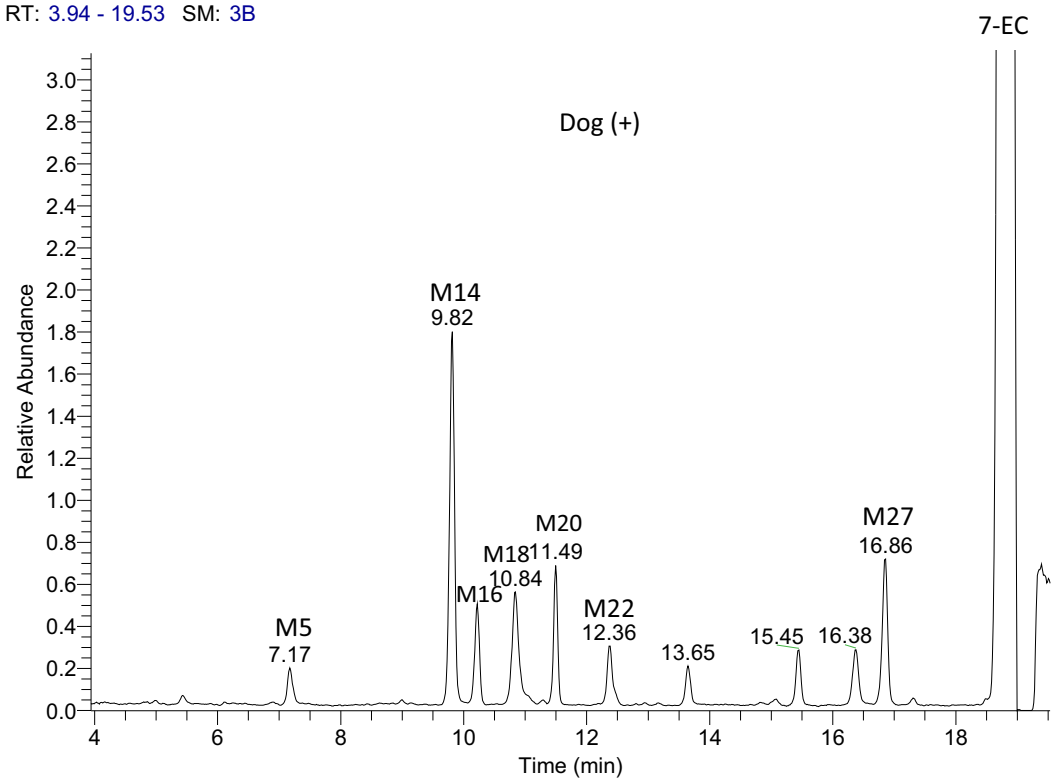

Fig. (3). Selected ion chromatograms of 7-ethoxycoumarin and its metabolites in dog hepatocytes in positive ion mode.

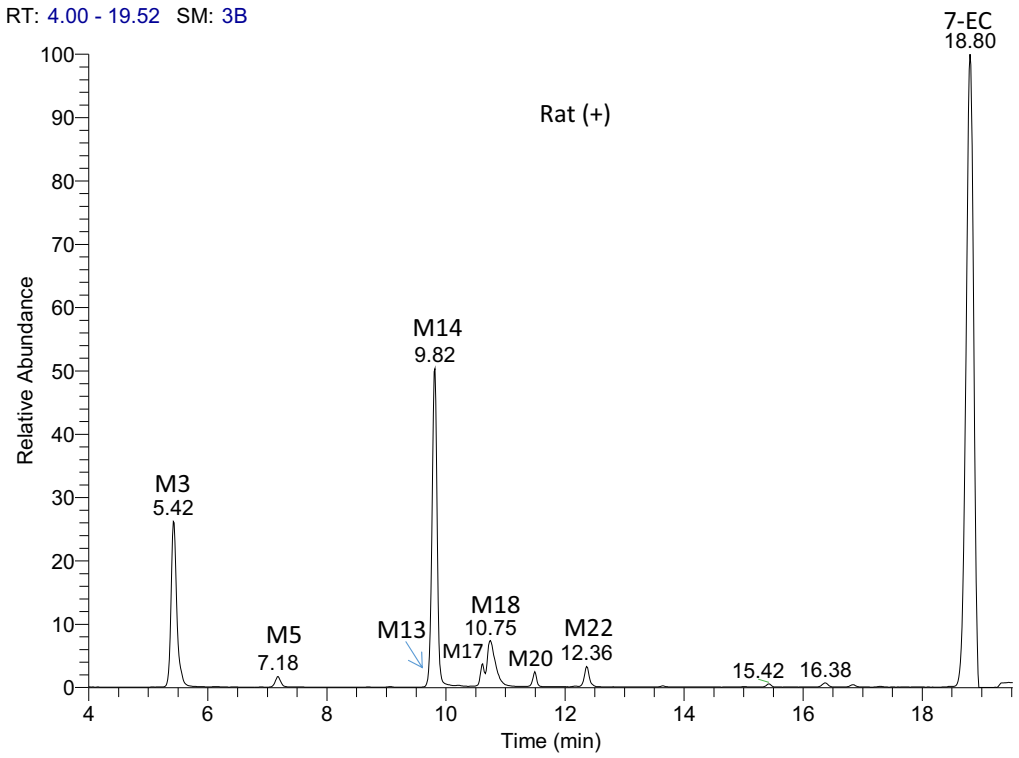

Fig. (4). Selected ion chromatograms of 7-ethoxycoumarin and its metabolites in rat hepatocytes in positive ion mode (note: M1 and M16 were not selected).

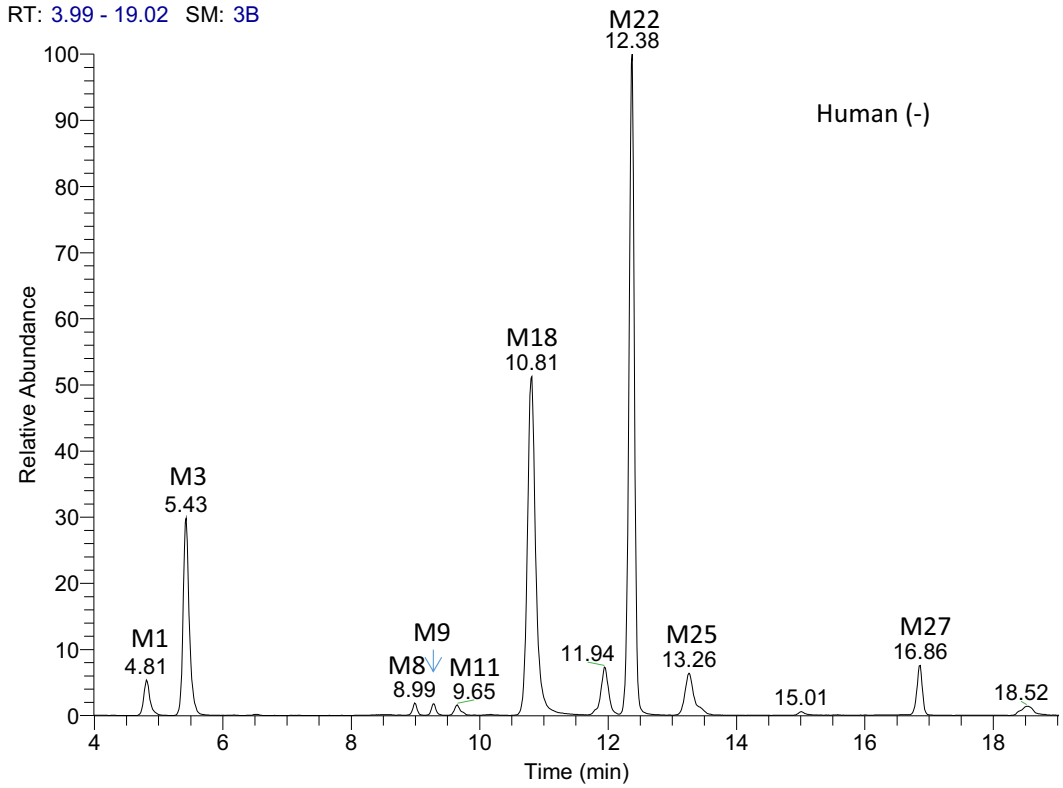

Fig. (5). Selected ion chromatograms of 7-ethoxycoumarin and its metabolites in human hepatocytes in negative ion mode.

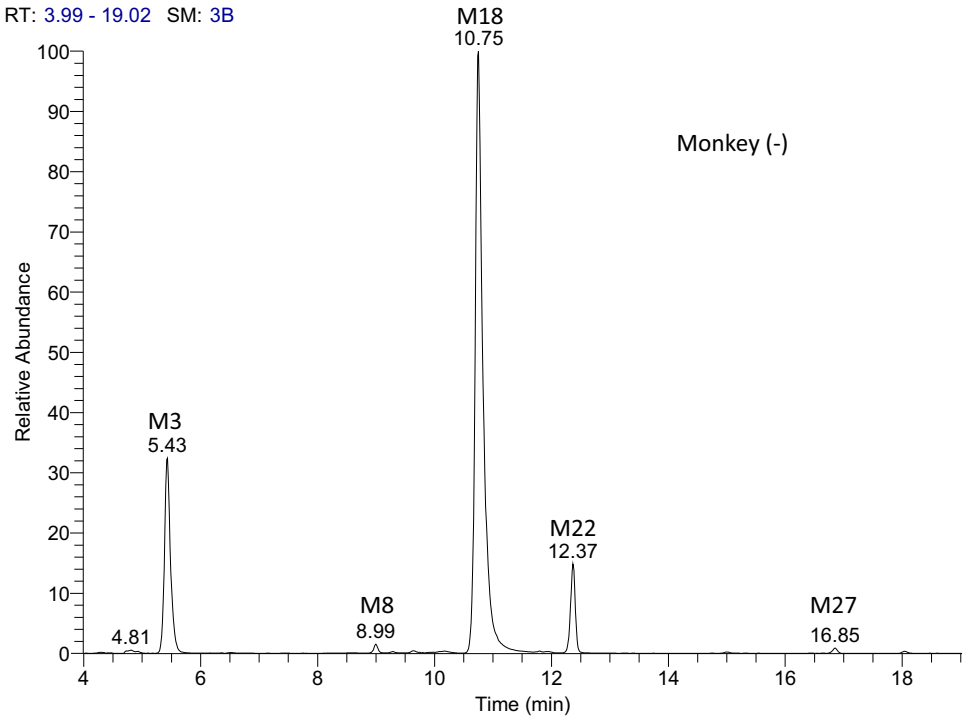

Fig. (6). Selected ion chromatograms of 7-ethoxycoumarin and its metabolites in monkey hepatocytes in negative ion mode.

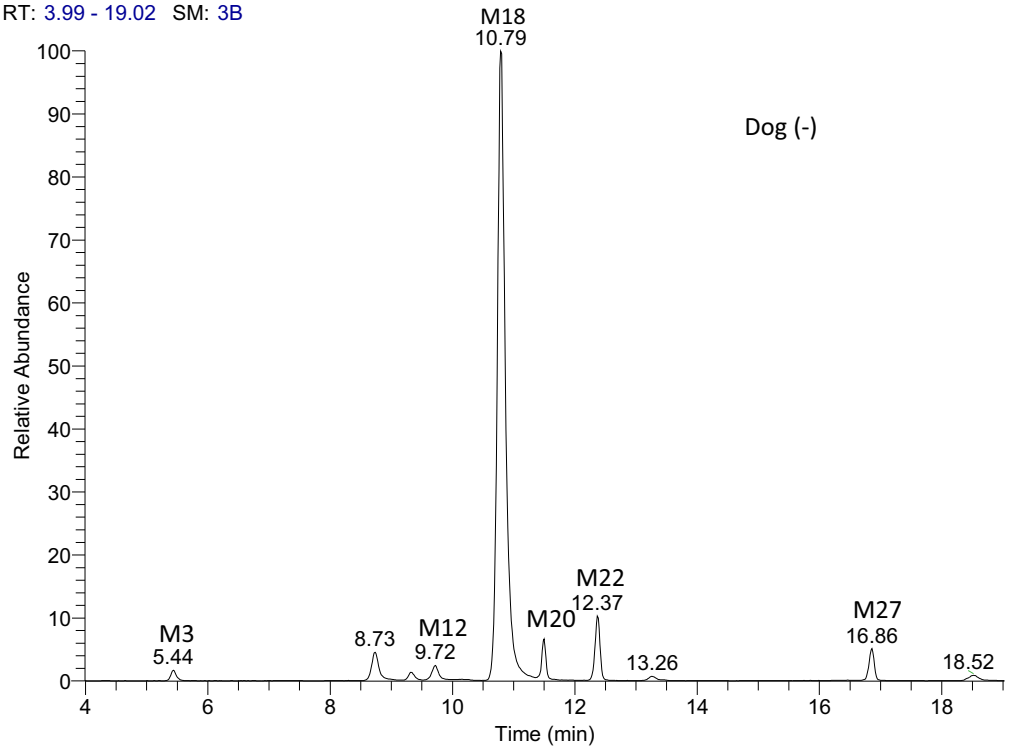

Fig. (7). Selected ion chromatograms of 7-ethoxycoumarin and its metabolites in dog hepatocytes in negative ion mode.

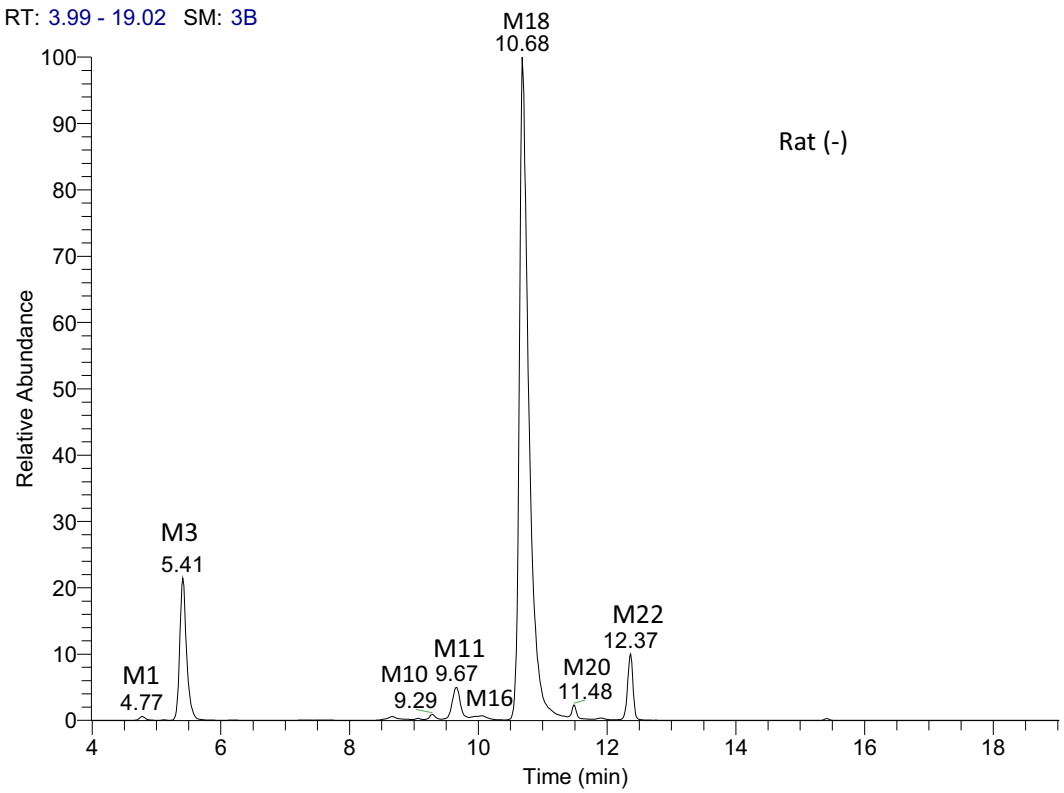

Fig. (8). Selected ion chromatograms of 7-ethoxycoumarin and its metabolites in rat hepatocytes in negative ion mode.

In human hepatocytes, O-deethylation, glucuronidation, sulfation, oxygenation, oxidative ring-opening, hydrogenation, glutathionation, dehydrogenation, cysteination, glucosidation, and hydrolysis were observed. In positive ion mode, 7-ethoxycoumarin was a dominant component accounting for 90.7% of the total abundance, while other components were metabolites accounting for 9.3% of the total abundance. Twenty one metabolites (M1, M3, M4, M5, M6, M7, M8, M13, M14, M16, M17, M18, M19, M20, M21, M22, M23, M24, M26, M27, and M28) were identified. As shown in Fig. (**1**), M14 was a metabolite as 7-hydoxycoumarin formed *via* O-deethylation, which was further biotransformed to M3 *via* glucuronidation, and M18 *via* sulfation. M5 was a metabolite *via* hydrolysis and mono-oxygenation. M13, M21, M24, M27, and M28 were metabolites *via* mono-oxygenation, in which M27 showed the highest abundance. M22 was also a metabolite *via* oxidative ring-opening and mono-oxygenation. It was tentatively identified as 4-ethoxy-2-hydroxy phenylacetic acid. Further biotransformation of M22 generated two glucuronides (M9 and M10) *via* glucuronidation, two glucosides (M8, M11) *via* glucosidation, and a sulfate (M25) *via* sulfation. M17 was a cysteine conjugate *via* glutamine and glycine hydrolysis of M20, which was a glutathione conjugate *via* glutathionation and dehydrogenation. Other minor metabolites included M1 *via* O-deethylation, mono-oxygenation and glucuronidation, M4 and M7 *via* O-deethylation and mono-oxygenation, M6 *via* mono-oxygenation and glucuronidation, M16 *via* hydrolysis, M19 *via* oxidative ring-opening, and M23 *via* oxidative ring-opening and hydrogenation. In negative ion mode, only 17 metabolites were detected, 7-ethoxycoumarin and some of the metabolites were not detected due to their inability for ionization *via* gas phase deprotonation, or very low concentrations. As shown in Fig. (**5**), M1, M3, M8, M9, M11, M18, M22, M25 and M27 exhibited relatively high abundances. Based on the mass spectrometric response, M1, M3, M5, M14, M16, M22 and M27 appeared to be major metabolites in human hepatocytes.

In monkey hepatocytes, O-deethylation, glucuronidation, sulfation, oxygenation, oxidative ring-opening, hydrogenation, glutathionation, dehydrogenation, cysteination, glucosidation, methylation, and hydrolysis were observed. In positive ion mode, 7-ethoxycoumarin was a major component accounting for 55.9% of the total abundance, while other components were metabolites accounting for 43.1% of the total abundance. Twenty-two metabolites (M1, M3, M4, M5, M6, M7, M8, M12, M13, M14, M15, M16, M17, M18, M19, M20, M21, M22, M23, M24, M26, M27, and M28) were identified. As shown in Fig. (**2**), M3, M5, M8, M14, M16, M18, M22 and M27 exhibited relatively high abundances. Other minor metabolites included M1, M4, M6, M7, M12, M13, M15, M17, M19, M20, M21, M23, M24, M26, and M28. In negative ion mode, only 15 metabolites were detected. As shown in Fig. (**6**), M3, M8, M18, M22 and M27 exhibited relatively high abundances. Based on the mass spectrometric response, M3, M5, M8, M13, M14, M16, M18, M22 and M27 appeared to be major metabolites in monkey hepatocytes.

In dog hepatocytes, O-deethylation, glucuronidation, sulfation, oxygenation, oxidative ring-opening, hydrogenation, glutathionation, dehydrogenation, cysteination, glucosidation, methylation, and hydrolysis were observed. In positive ion mode, 7-ethoxycoumarin was a dominant component accounting for 96.6% of the total abundance, while other

components were metabolites accounting for 3.4% of the total abundance. Twenty metabolites were identified. As shown in Fig. (**3**), M5, M14, M16, M18, M20, M22 and M27 exhibited relatively high abundances. Other minor metabolites included M1, M3, M6, M7, M12, M13, M15, M17, M19, M21, M23, M24, and M28. In negative ion mode, only 14 metabolites were detected. As shown in Fig. (**7**), M3, M12, M18, M20, M22 and M27 exhibited relatively high abundances. Based on the mass spectrometric response, M14, M16, M18, M20 and M27 appeared to be major metabolites in dog hepatocytes.

In rat hepatocytes, O-deethylation, glucuronidation, sulfation, oxygenation, oxidative ring-opening, hydrogenation, glutathionation, dehydrogenation, cysteination, glucosidation, methylation, and hydrolysis were observed. In positive ion mode, 7-ethoxycoumarin was a major component accounting for 58.5% of the total abundance, while other components were metabolites accounting for 41.5% of the total abundance. Twenty-two metabolites were identified. As shown in Fig. (**4**), M3, M5, M14, M17, M18, M20, and M22 exhibited relatively high abundances. Other minor metabolites included M1, M2, M4, M6, M7, M12, M13, M15, M17, M19, M21, M23, M24, and M28. In negative ion mode, only 17 metabolites were detected. As shown in Fig. (**8**), M3, M11, M18, M20 and M22 exhibited relatively high abundances. Based on the mass spectrometric response, M1, M3, M5, M13, M14, M16, M17, M18, M20, and M22 appeared to be major metabolites in rat hepatocytes.

Species differences across human, monkey, dog, and rat hepatocytes in the metabolism of 7-ethoxycoumarin were observed. 7-Ethoxycoumarin was more stable in human and dog hepatocytes than in monkey and rat hepatocytes. It showed that O-deethylation was a common major pathway across four species. Other different major pathways were obvious (Figs. **1-4**). In human hepatocytes, oxidative ring-opening/oxygenation, hydrolysis and oxygenation were major pathways. In monkey hepatocytes, 7-hydroxycoumarin glucuronidation was a major pathway. In dog hepatocytes, 7-hydroxycoumarin sulfation, glutathionation and dehydrogenation, hydrolysis, and oxygenation were major pathways. In rat hepatocytes, 7-hydroxycoumarin glucuronidation was a major pathway.

3.2. Structural Elucidation of Metabolites

Metabolites were further confirmed and characterized using LC-MS^2. MS/MS spectrum of 7-ethoxycoumarin is shown in Fig. (**9**). MS/MS spectra of M3, M14, M17, M18, M20, and M22 in positive ion mode are presented in Figs. (**10-15**). Possible fragmentation pathways and their fragment ion strucures of M14, M17, M20 and M22 are proposed in Schemes **3-6**. MS/MS spectra of M8, M9, and M25 in negative ion mode are presented in Figs. (**16-18**). Their possible fragmentation pathways and their fragment ion strucures are proposed in Schemes **7-9**. The structures of detected metabolites were elucidated by the comparative analysis of fragment ions between the parent (Fig. **9**) and individual metabolites.

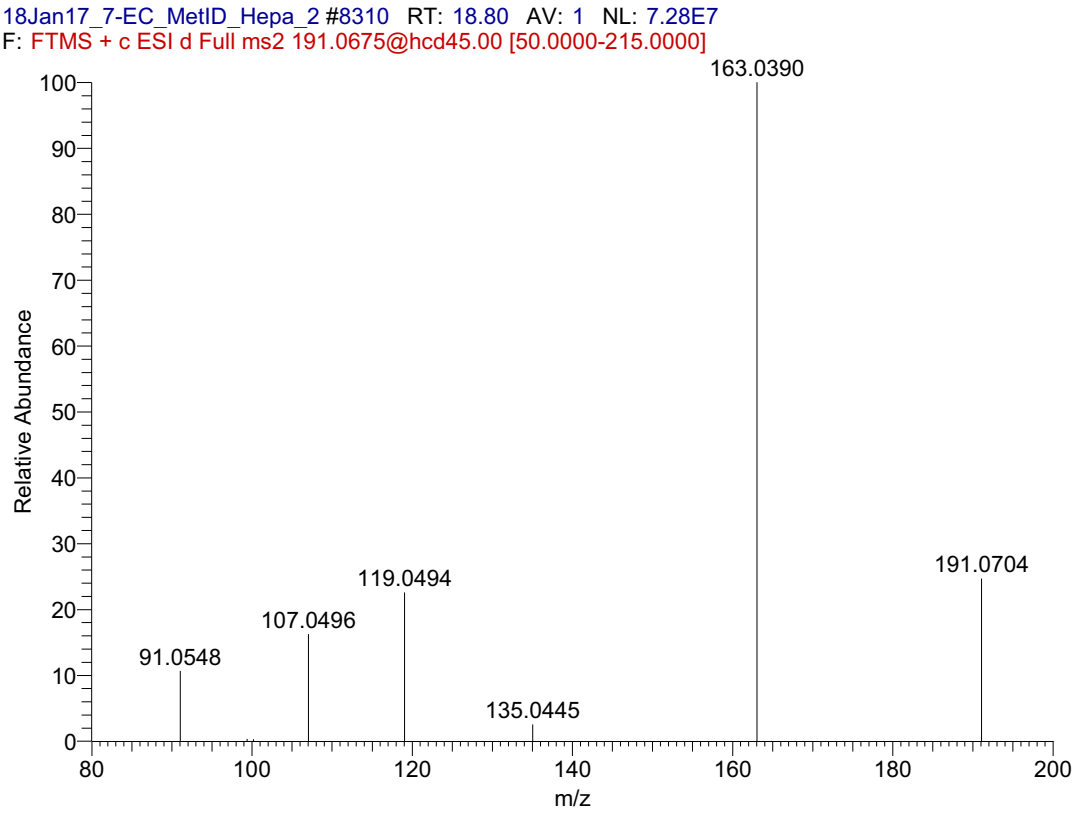

Fig. (9). MS/MS mass spectrum of 7-exthoxycoumarin (*m/z* = 191.0703) in positive ion mode.

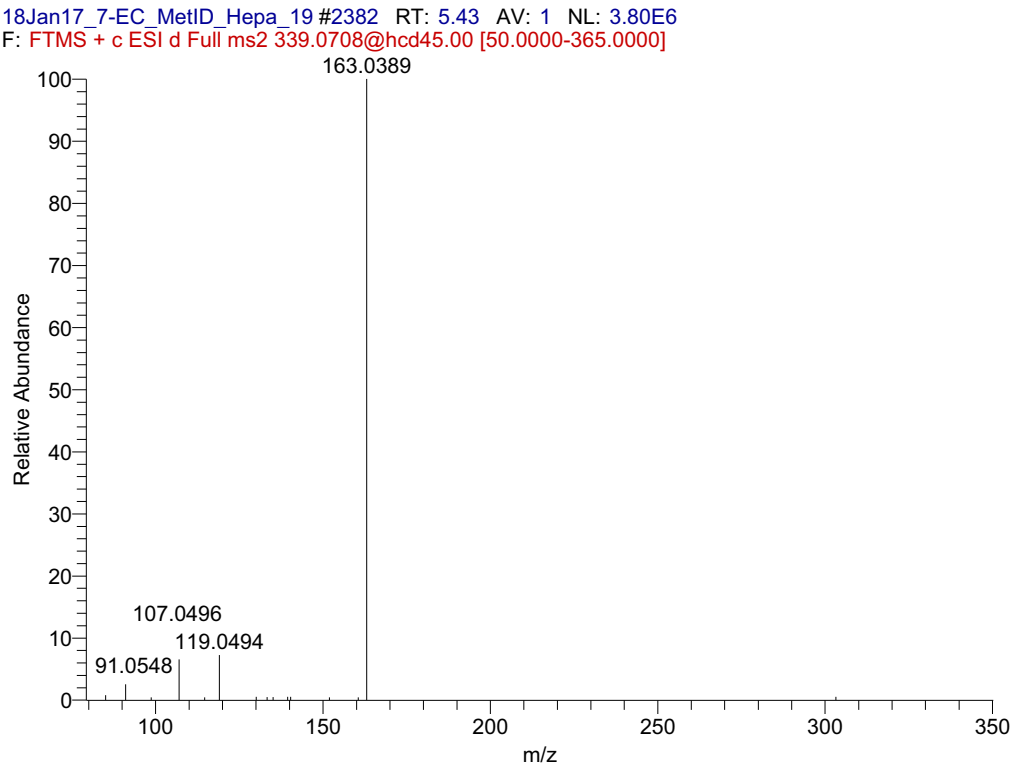

Fig. (10). MS/MS mass spectrum of M3 (coumarin-7-O-glucuronide) (*m/z* = 339.0711) in positive ion mode.

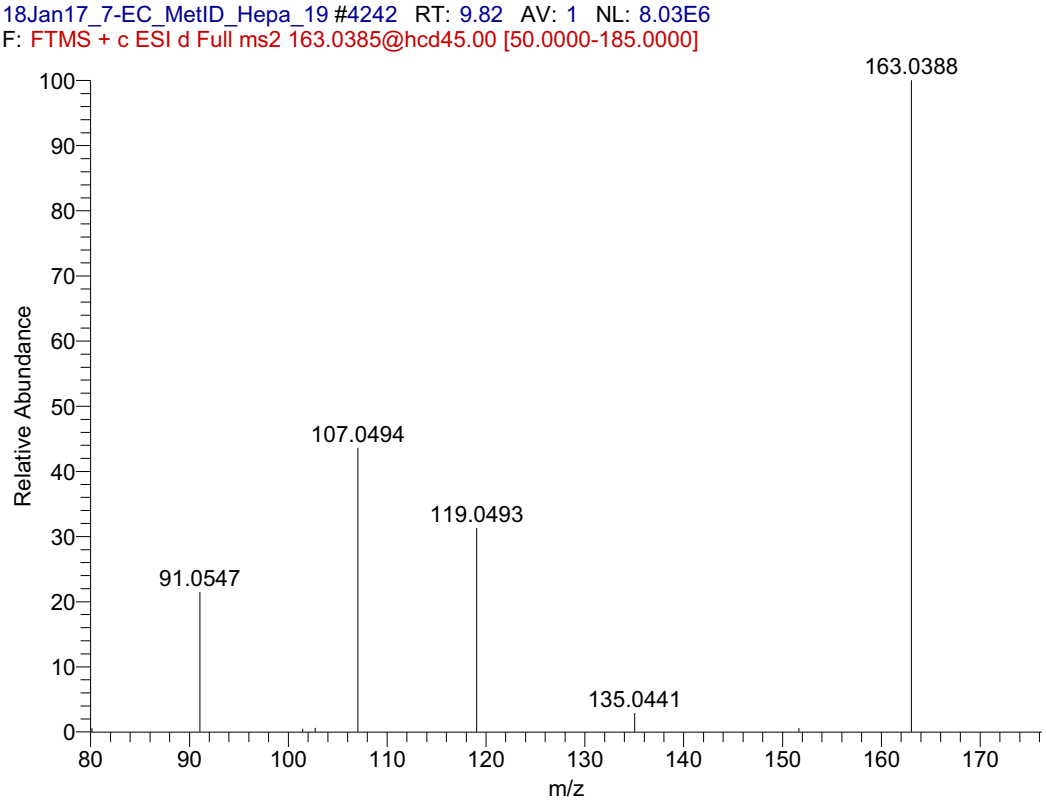

Fig. (11). MS/MS mass spectrum of M14 (7-hydroxycoumarin) (*m/z* = 163.0390) in positive ion mode.

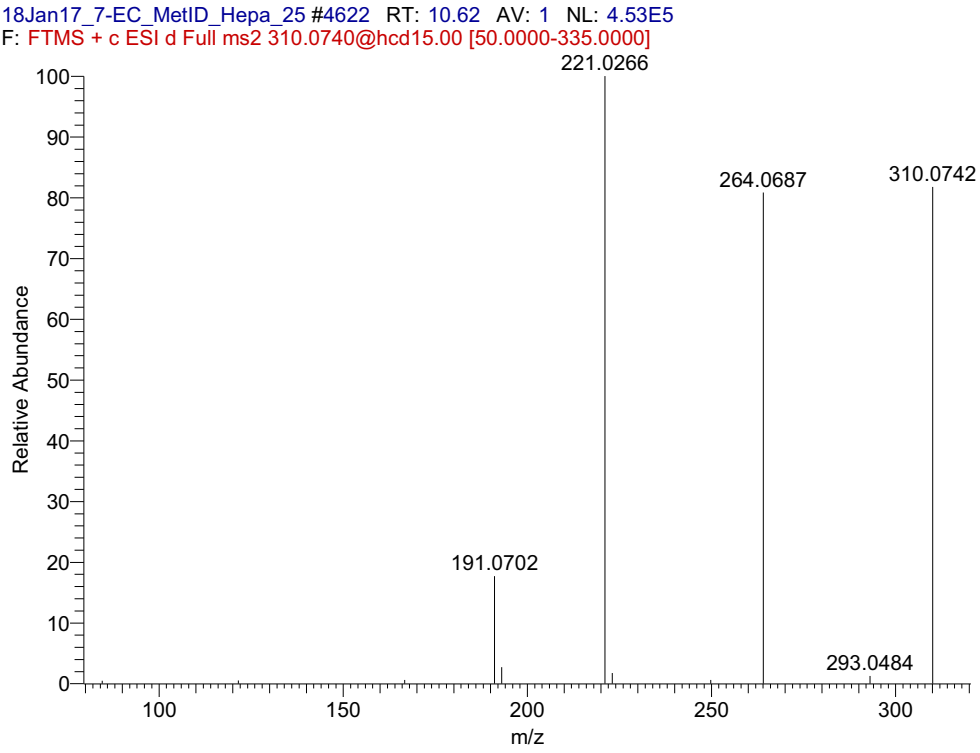

Fig. (12). MS/MS mass spectrum of M17 (*m/z* = 310.0744) in positive ion mode.

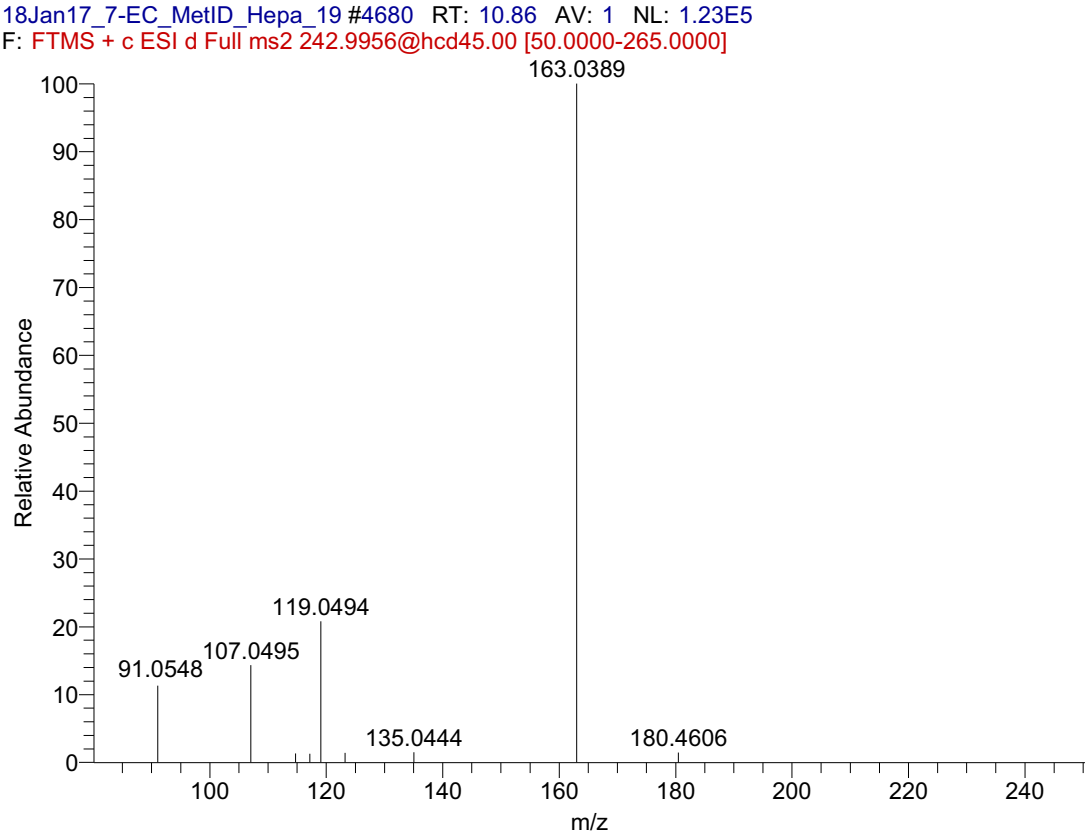

Fig. (13). MS/MS mass spectrum of M18 (coumarin-7-O-sulfate) (*m/z* = 242.9959) in positive ion mode.

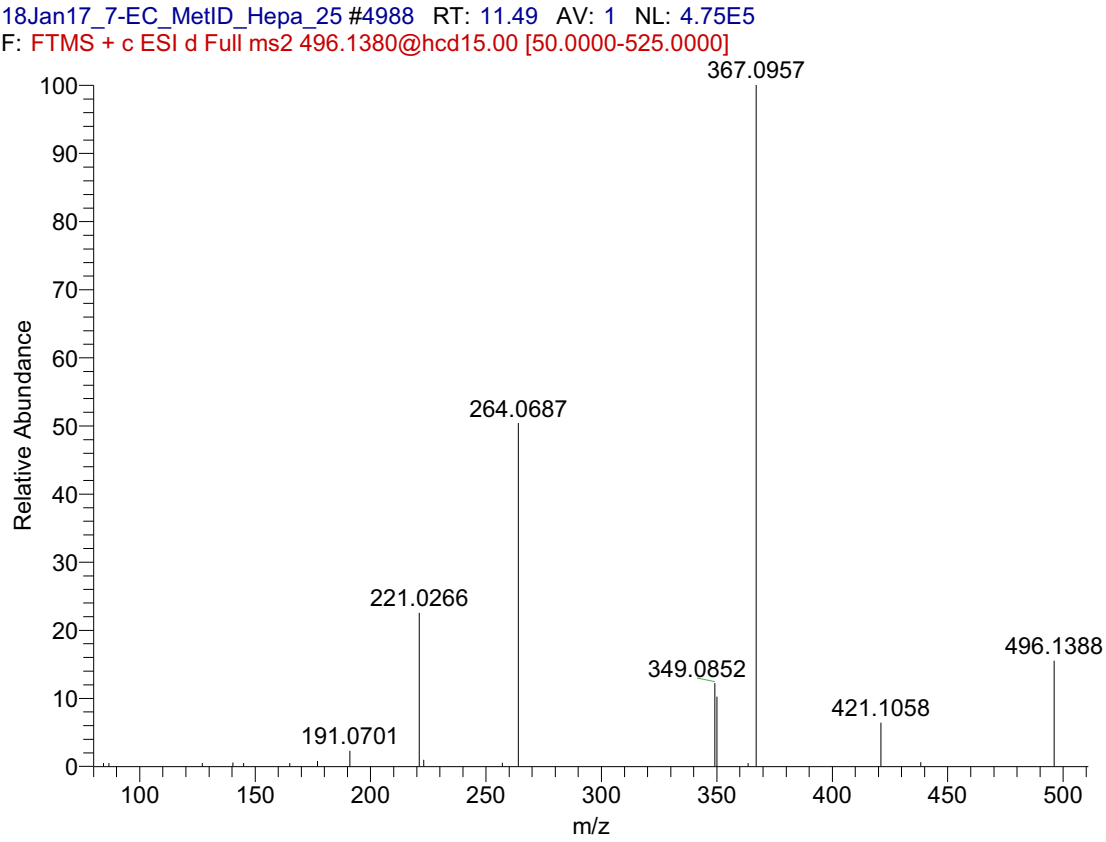

Fig. (14). MS/MS mass spectrum of M20 (*m/z* = 496.1384) in positive ion mode.

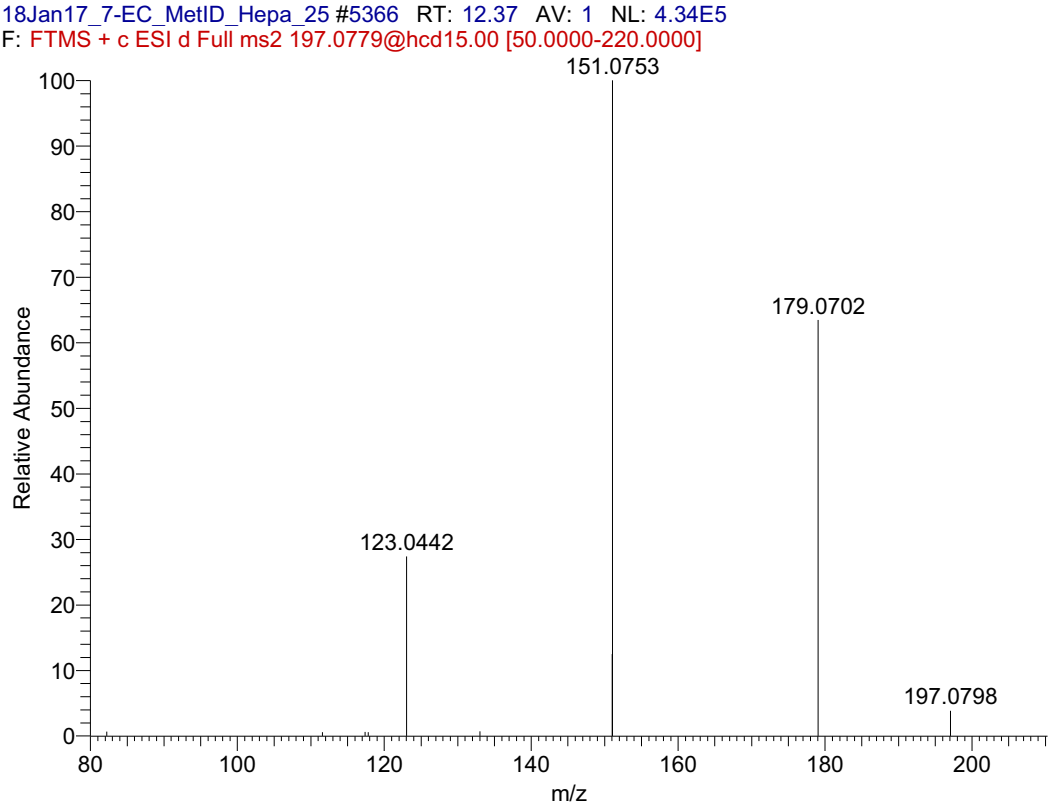

Fig. (15). MS/MS mass spectrum of M22 (*m/z* = 197.0808) in positive ion mode.

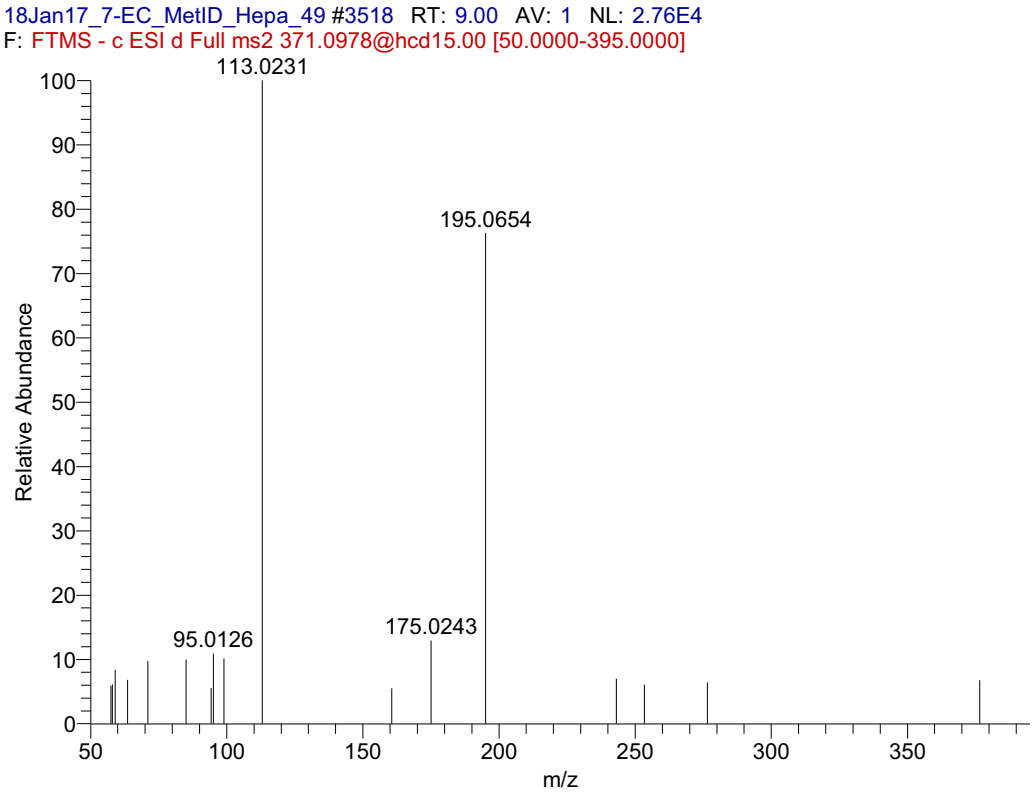

Fig. (16). MS/MS mass spectrum of M8 (*m/z* = 371.0983) in negative ion mode.

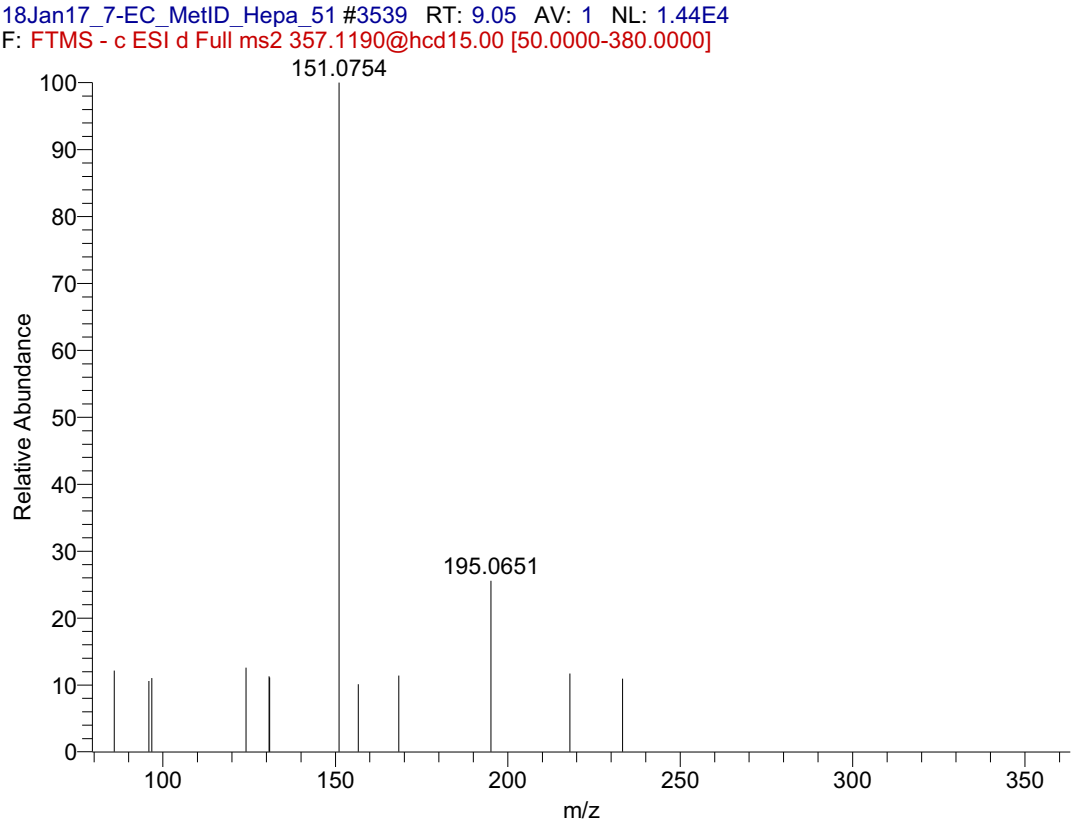

Fig. (17). MS/MS mass spectrum of M9 (*m/z* = 357.1191) in negative ion mode.

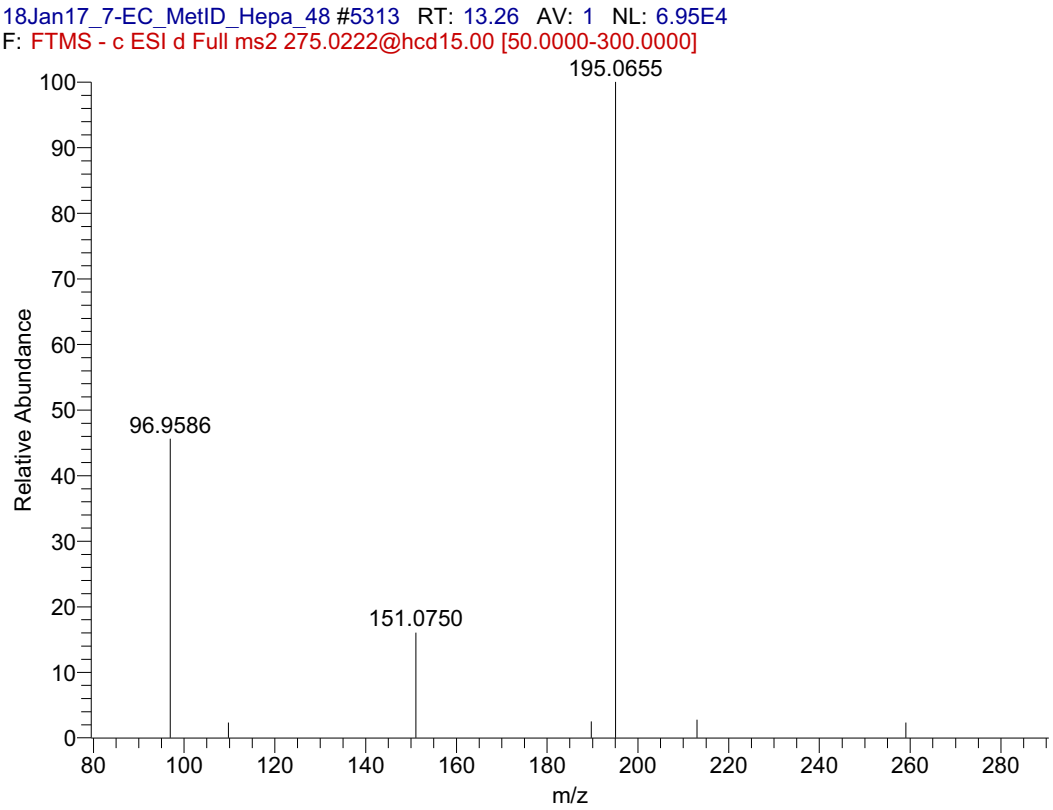

Fig. (18). MS/MS mass spectrum of M25 (*m/z* = 275.0230) in negative ion mode.

Possible fragmentation pathways of 7-ethoxycoumarin are proposed in Scheme **2**. The fragment ion *m/z* = 163.1 of 7-ethoxycoumarin was formed *via* a neutral C_2H_4 loss, and further produced other fragment ions, *m/z* = 135.0, 119.0, 107.0, 91.0. These fragment ions were also detected from MS/MS spectrum of M14 (7-hydroxycoumarin), as shown in Scheme **3**, which were identical between 7-ethoxycoumarin and 7-hydroxycoumarin. 7-Hydroxycoumarin as a metabolite standard of M14 prepared in 10% acetonitrile/0.1% formic acid showed the same retention time and fragmentation pattern (data not shown) as M14. This confirmed that M14 was 7-hydroxycoumarin. M14 was further oxygenated to dihydroxycoumarins (M4 and M7). Both M4 and M7 produced a key fragment ion *m/z* = 123.0 (107.0 + 16) due to a mass shift from *m/z* = 107.0. This indicated that an oxygen atom was added to the benzene part, which was supported by proposed fragment ions: *m/z* = 151.0 *via* CO loss, and 133.0 *via* HCOOH loss. A methylated metabolite M15 from M4 or M17 was detected and its MS/MS fragment ions were supported by proposed fragment ions (data not shown). There was an oxidative ring-opening pathway to produce M19 (an aldehyde), which was further oxygenated to a carboxylic acid (M22), or dehydrogenated to an alcohol (M23). Fig. (**15**) shows MS/MS spectrum of M22 in positive ion mode. Three abundant fragment ions *m/z* = 179.1, 151.1 and 123.0 were produced by a water loss, a formic acid loss, and formic acid and ethylene losses, respectively, and supported by proposed fragment ions (Scheme **6**). Further biotransformation of M22 produced M25 *via* sulfation, M8 and M11 *via* glucosidation, and M9 and M10 *via* glucuronidation. Interestingly, M8 - M11 and M25 were only detected in negative ion mode. As shown in Figs. (**16**-**18**) for MS/MS spectra of

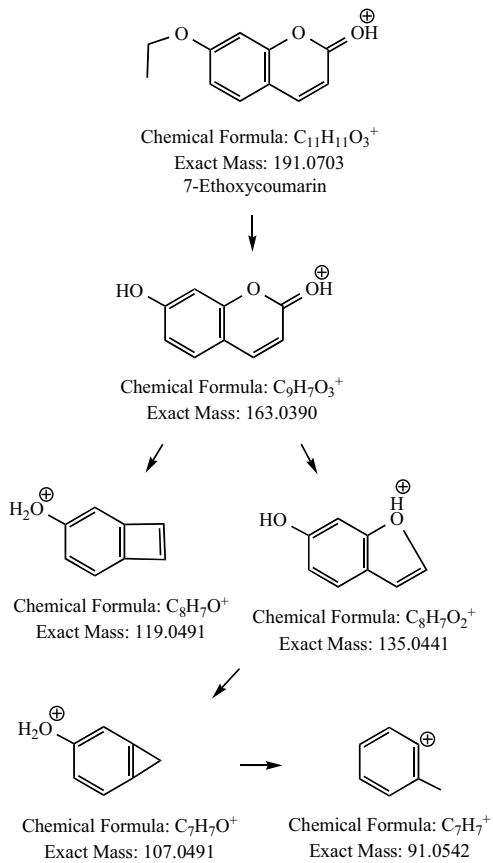

Scheme 2. Proposed fragmentation pathways of 7-exthoxycoumarin (*m/z* = 191.0703) in positive ion mode.

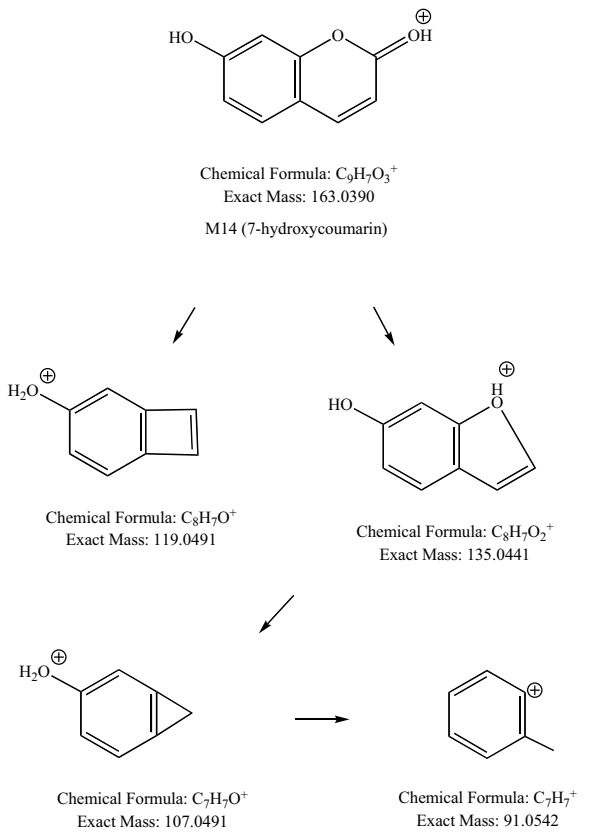

Scheme 3. Proposed fragmentation pathways of M14 (7-hydroxycoumarin) (*m/z* = 163.0390) in positive ion mode.

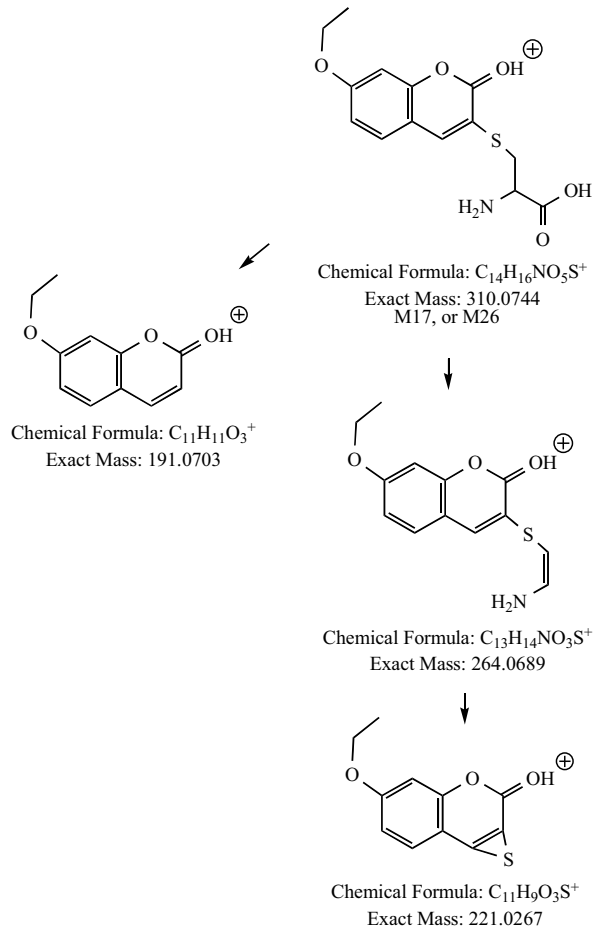

Scheme 4. Proposed fragmentation pathways of M17 (*m/z* = 310.0744) in positive ion mode.

M8, M9 and M25, besides characteristic neutral 176, 162 and 80 losses as an indicator of glucuronide, glucoside and sulfate, respectively, there were two more key fragment ions *m/z* = 195.1 and 151.1 which were produced from M8, M9 and M25. Fragment ions of M8, M9, and M25 were further supported by proposed fragment ions, as shown in Schemes **7-9**. For five mono-oxygenated metabolites (M13, M21, M24, M27 and M28), MS/MS fragment analyses with a fragment ion *m/z* = 123.0 due to a mass shift from *m/z* = 107.0 suggest that the oxygenated site of M21, M24 and M28 may be on the benzene ring (data not shown). Hydrolyzed metabolite M16 had several key fragment ions *m/z* = 191.1 *via* H_2O loss, and 163.1 *via* H_2O and C_2H_4 losses, and were supported by proposed fragment ions. Hydrolyzed and mono-oxygenated metabolite M5 had several key fragment ions *m/z* = 207.1 *via* H_2O loss, 179.1 *via* CO loss, and 163.1, 135.0, 107.0, and were supported by proposed fragment ions.

A glucuronide conjugate metabolite has a unique and dominant fragmentation pathway by a neutral glucuronic acid residual loss of 176 amu at MS/MS. M1, M3, M6, M8, and M11 were glucuronides giving a neutral 176 loss. A representative MS/MS spectrum from M3 (*m/z* = 339.1) is shown in Fig. (**10**), having a fragment ion m/z 163 formed *via* a neutral 176 loss from *m/z* = 339.1. This was supported by proposed fragment ions (data not shown). A glucoside conjugate metabolite has a unique and dominant fragmentation pathway by a neutral glucose residual loss of 162 amu at MS/MS. M2, M9, and M10 were glucoside conjugates giving a neutral 162 loss. A representative MS/MS spectrum from M9 (*m/z* = 357.1) is shown in Fig. (**17**), having a fragment ion *m/z* = 195.0 formed *via* a neutral 162 loss from *m/z* = 357.1. This was supported by proposed fragment ions (Scheme **8**). A sulfate conjugate metabolite has a unique and dominant fragmentation pathway by a neutral SO_3 loss of 80 amu at MS/MS. M12, M18 and M25 were sulfates giving a neutral 80 loss. Representative MS/MS spectra from M18 (*m/z* = 243.0) and M25 (*m/z* = 275.0) are shown in Fig. (**13**) and in Fig. (**18**), respectively, having a fragment ion *m/z* = 163.0 and 195.1 formed *via* a neutral 80 loss from *m/z* = 243.0 and 275.0, respectively. This was supported by proposed fragment ions of M18 and M25. The fragmentation pathway of M25 is shown in Scheme **9**.

Interestingly, one glutathione conjugate M20, and two cysteine conjugates M17 and M26 were detected across four species. MS/MS spectrum of M20 in positive ion mode is shown in Fig. (**14**). Fragment ions *m/z* = 421.1, and 367.1 were detected *via* a neutral loss of glycine (75) and glutamine residue (129), respectively. Neutral 129 and 75 losses are common indicators for glutathione conjugates. This was further supported by proposed fragment ions (Scheme **5**). MS/MS spectrum of M17 in positive ion mode is shown in Fig. (**12**). Fragment ions *m/z* = 264.1, 221.0 and 191.1 were detected and further supported by proposed fragment ions (Scheme **4**).

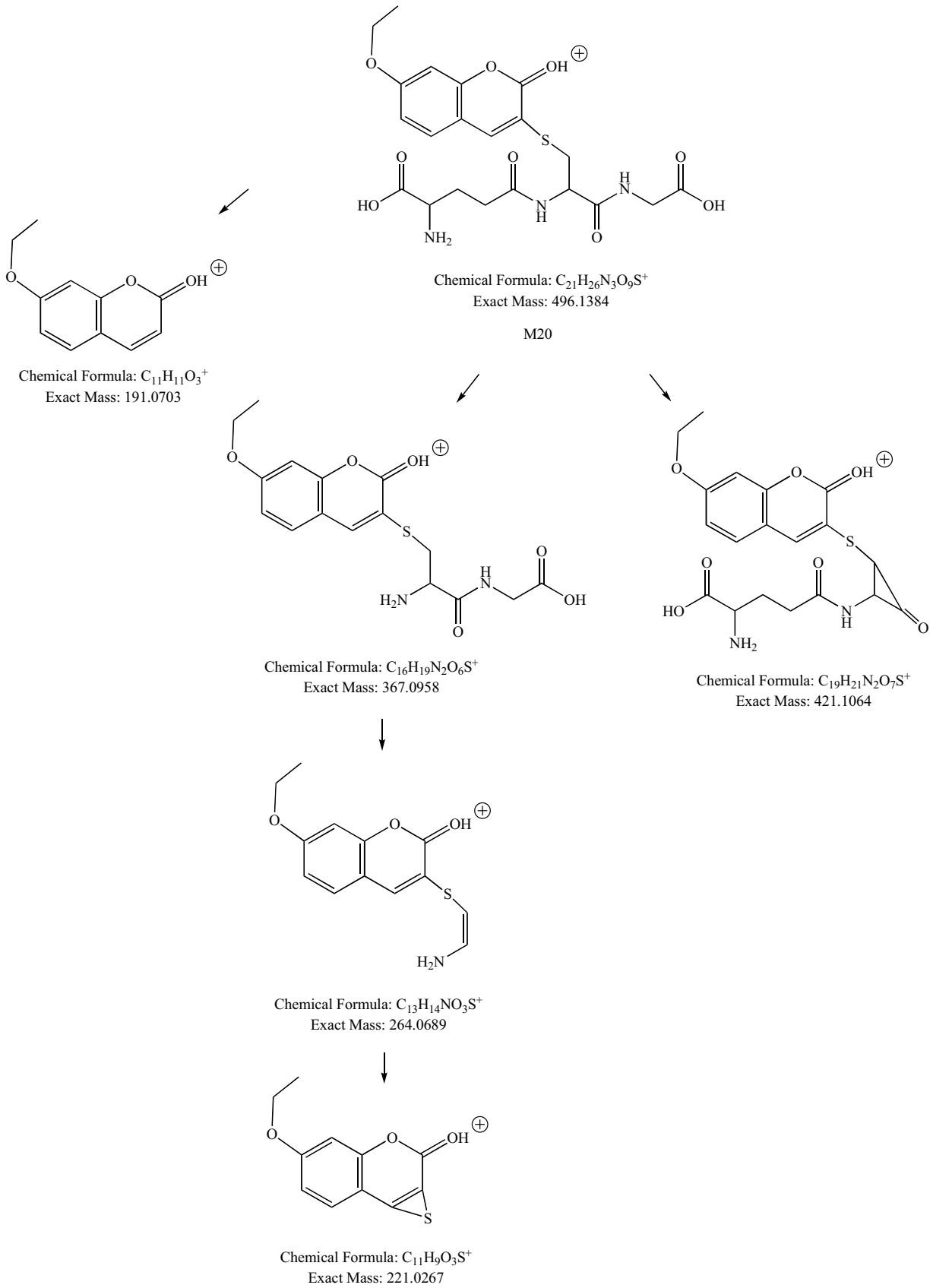

Scheme 5. Proposed fragmentation pathways of M20 (*m/z* = 496.1384) in positive ion mode.

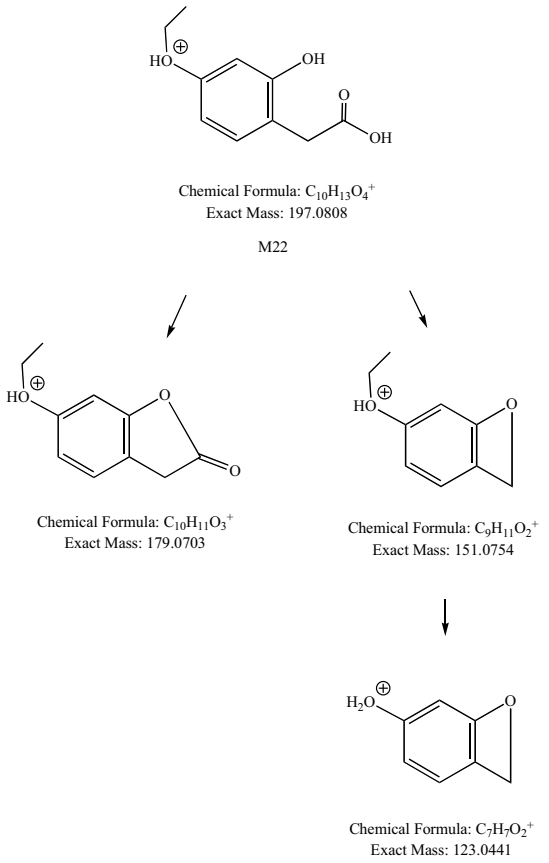

Scheme 6. Proposed fragmentation pathways of M22 (*m/z* = 197.0808) in positive ion mode.

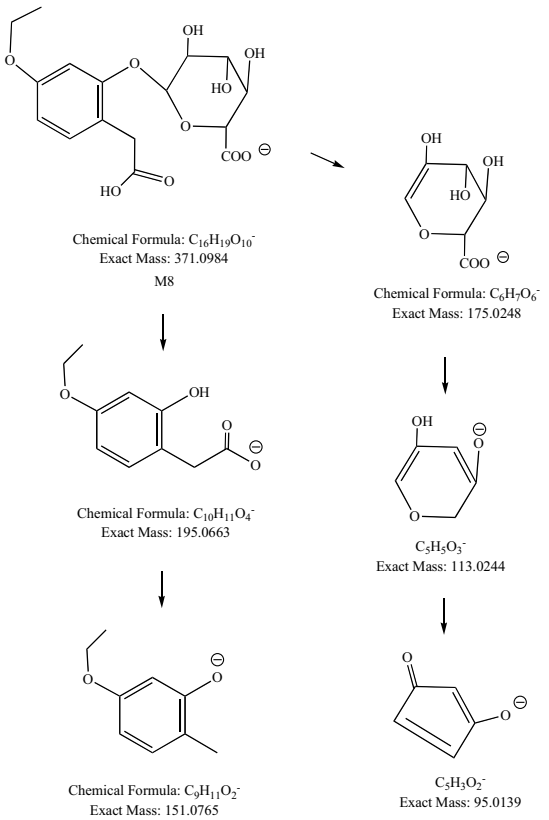

Scheme 7. Proposed fragmentation pathways of M8 (*m/z* = 371.0983) in negative ion mode.

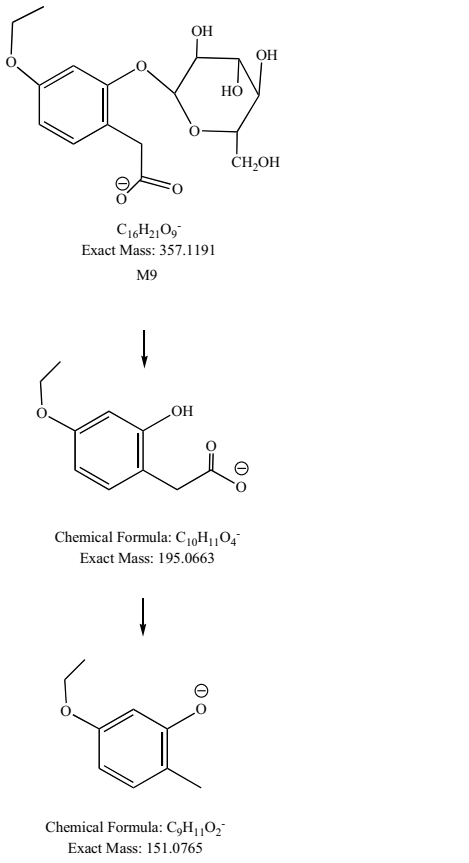

Scheme 8. Proposed fragmentation pathways of M9 (*m/z* = 357.1191) in negative ion mode.

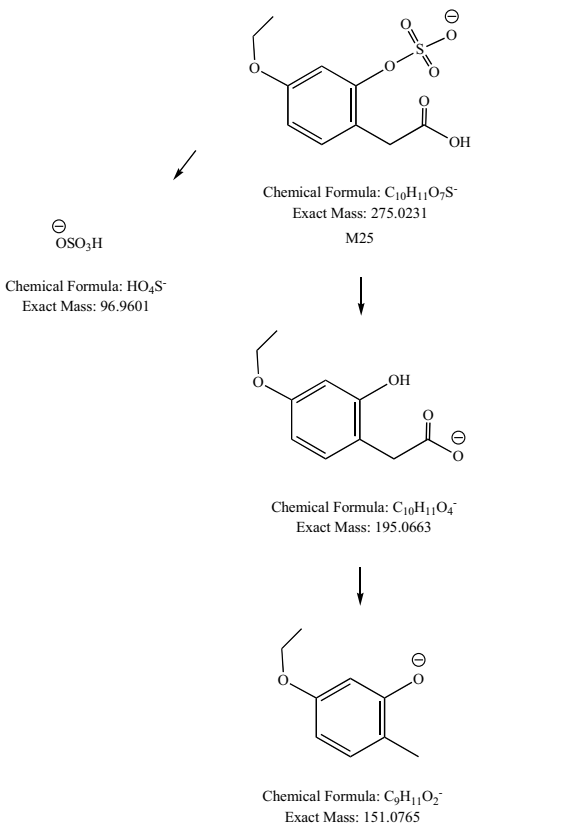

Scheme 9. Proposed fragmentation pathways of M25 (*m/z* = 275.0230) in negative ion mode.

It should be pointed out that these new metabolites were tentatively identified. They need to be further identified and confirmed using additional analytical techniques such as NMR with isolated and concentrated enough samples, or by synthesizing proposed metabolite standards for LC-MS/MS comparisons between identified ones and synthesized ones.

3.3. Discussion

Metabolism of 7-ethoxycoumarin has been studies in human liver slices [12] and microsomes [11, 13]. O-deethylation, and its subsequential glucuronidation and sulfation were reported with three dominant metabolites, 7-hydroxycoumarin, coumarin-7-O-glucuronide, and coumarin-7-O-sulfate. In human liver microsomes in the presence of β-NADPH and UGT-GA, 3-hydroxy-7-ethoxycoumarin and 7-ethoxycoumarin-3-O-glucurinde besides 7-hydroxycoumarin and coumarin-7-O-glucuronide were identified and confirmed by NMR [13]. Overall, five metabolites of 7-ethoxycoumarin (7-hydroxycoumarin, coumarin-7-O-glucuronide, coumarin-7-O-sulfate, 3-hydroxy-7-ethoxycoumarin, and 7-ethoxycoumarin-3-O-glucurinde) in *in vitro* human systems were reported. In the present study, five mono-oxygenated metabolites (M13, M21, M24, M27 and M28) were detected, and 3-hydroxy-7-ethoxycoumarin may be one of the five. M6 was only a detected metabolite *via* mono-oxygenation and glucuronidation, and may be considered as 7-ethoxycoumarin-3-O-glucurinde. Sixteen metabolites were newly identified.

Two studies on metabolism of 7-ethoxycoumarin in *in vitro* monkey systems were reported. In Cynomolgus monkey liver slices, 7-hydroxycoumarin, coumarin-7-O-glucuronide, and coumarin-7-O-sulfate were reported [12]. Marmoset lung CYP450 2F1 catalyzed biotransformation of 7-ethoxycoumarin was reported to produce 7-hydroxycoumarin, and dihydroxy-7-ethoxycoumarin [14]. Overall, four metabolites of 7-ethoxycoumarin (7-hydroxycoumarin, coumarin-7-O-glucuronide, coumarin-7-O-sulfate, and dihydroxy-7-ethoxycoumarin) in *in vitro* monkey systems were reported. In the present study, no dihydroxy-7-ethoxycoumarin was detected, but 19 metabolites were newly identified.

A study on metabolism of 7-ethoxycoumarin in the *in vitro* dog system was reported [15]. In dog liver slices, coumarin-7-glucuronide, and coumarin-7-sulfate were major metabolites with a small extent of 4-ethoxy-2-hydroxyphenylacetic acid. Overall, 3 metabolites of 7-ethoxycoumarin (coumarin-7-O-glucuronide, coumarin-7-O-sulfate, and 4-ethoxy-2-hydroxyphenylacetic acid) in the *in vitro* dog system were reported. In the present study, 16 metabolites were newly identified.

Metabolism of 7-ethoxycoumarin has been widely studied in rat liver slices [12, 17], lung slices [16], skin strips [18], perfused intestinal loop [19], rat brain [20], and hepatocytes [21, 22]. It was reported that 7-hydroxycoumarin, coumarin-7-O-glucuronide, and coumarin-7-O-sulfate were identified in rat liver slices [12, 16, 17], lung [16], and skin [18]. Among them, coumarin-7-O-sulfate was a major conjugate [12, 16-18, 21], or had a comparable extent with coumarin-7-glucuronide in the intestine [19]. Only 7-hydroxycoumarin was identified in rat brain [20]. Other minor unknown metabolites were also detected in rat lung [16]. 7-Ethoxycoumarin was found to link with glutathione reduction in injured rat hepatocytes [22]. Coumarin-7-O-glucuronide and coumarin-7-O-sulfate were also identified in serum and urine following single oral administration to male SD rats [23]. Overall, three metabolites of 7-ethoxycoumarin (7-hydroxycoumarin, coumarin-7-O-glucuronide, and coumarin-7-O-sulfate) in *in vitro* and *in vivo* rat systems were reported. In the present study, 19 metabolites were newly identified.

In other *in vitro* systems, O-deethylation and subsequential glucuronidation and sulfation were found as major metabolic pathways. In Guinea pig liver slices [12] and pig ear skin [24], 7-hydroxycoumarin, coumarin-7-O-glucuronide, and coumarin-7-O-sulfate were identified, in which coumarin-7-O-sulfate was a major conjugate. 4-ethoxy-2-hydroxyphenylacetic acid and coumarin-7-O-glucuronide were also reported as major metabolites in Guinea pig liver slices [15]. In mouse liver slices [12] and skin [18], 7-hydroxycoumarin, coumarin-7-O-glucuronide, and coumarin-7-O-sulfate were identified, in which coumarin-7-O-sulfate was a major conjugate. In rabbit eyes [25], 7-hydroxycoumarin was identified. In fertile hen's eggs [26], 7-hydroxycoumarin, coumarin-7-O-glucuronide, and coumarin-7-O-sulfate were identified. In perfused trout liver [27], coumarin-7-O-glucuronide and a trace amount of coumarin-7-O-sulfate were identified.

Two microbial metabolites were identified as 7-hydroxycoumarin, 7-hydroxy-6-methoxycoumarin in *Streptomyces griseus* and *peucetius* [28, 29]. In *Escherichia coli* [30], when incubated with bacterial CYP450 102A1, 7-ethoxycumarin was biotransformed to 7-hydroxycoumarin and 3-hydroxy-7-ethoxycoumarin [31, 32].

Overall, comparisons between this study and literature reports in humans, monkeys, dogs and rats indicated that approximately 16 new metabolites were formed *via* additional metabolic pathways of oxidative ring-opening, hydrogenation, glutathionation, dehydrogenation, cysteination, glucosidation, methylation, and hydrolysis, which were not reported previously. It should be pointed out that new metabolites identified in this study may result from differences of test systems (hepatocytes *vs*. liver slides or liver microsomes), experimental conditions such as 7-ethoxycoumarin and drug-metabolizing enzyme concentrations, and bioanalytical technique (high resolution MS/MS *vs*. conventional MS/MS) between this study and literature ones. A higher resolution and sensitivity MS/MS detector in this study may be one of the reasons.

Metabolism of coumarin has been widely studied [1]. Coumarin underwent CYP enzymes dependent 3,4-epoxidation to generate a reactive coumarin epoxide. 2-hydroxyphenylacetaldehyde (a hepatotoxic intermediate), 2-hydroxyphenylethanol, and 2-hydroxyphenylacetic acid were further formed. Bioactivation of coumarin *via* 3,4-epoxidation was reported to be significantly species dependent. 3,4-epoxidation pathway appeared to be the major route in rats and mice, but not in humans. The present data analysis of metabolites and metabolic pathways in four species suggests that 7-ethoxylcoumarin may own a similar epoxidation pathway for oxidative ring-opening and

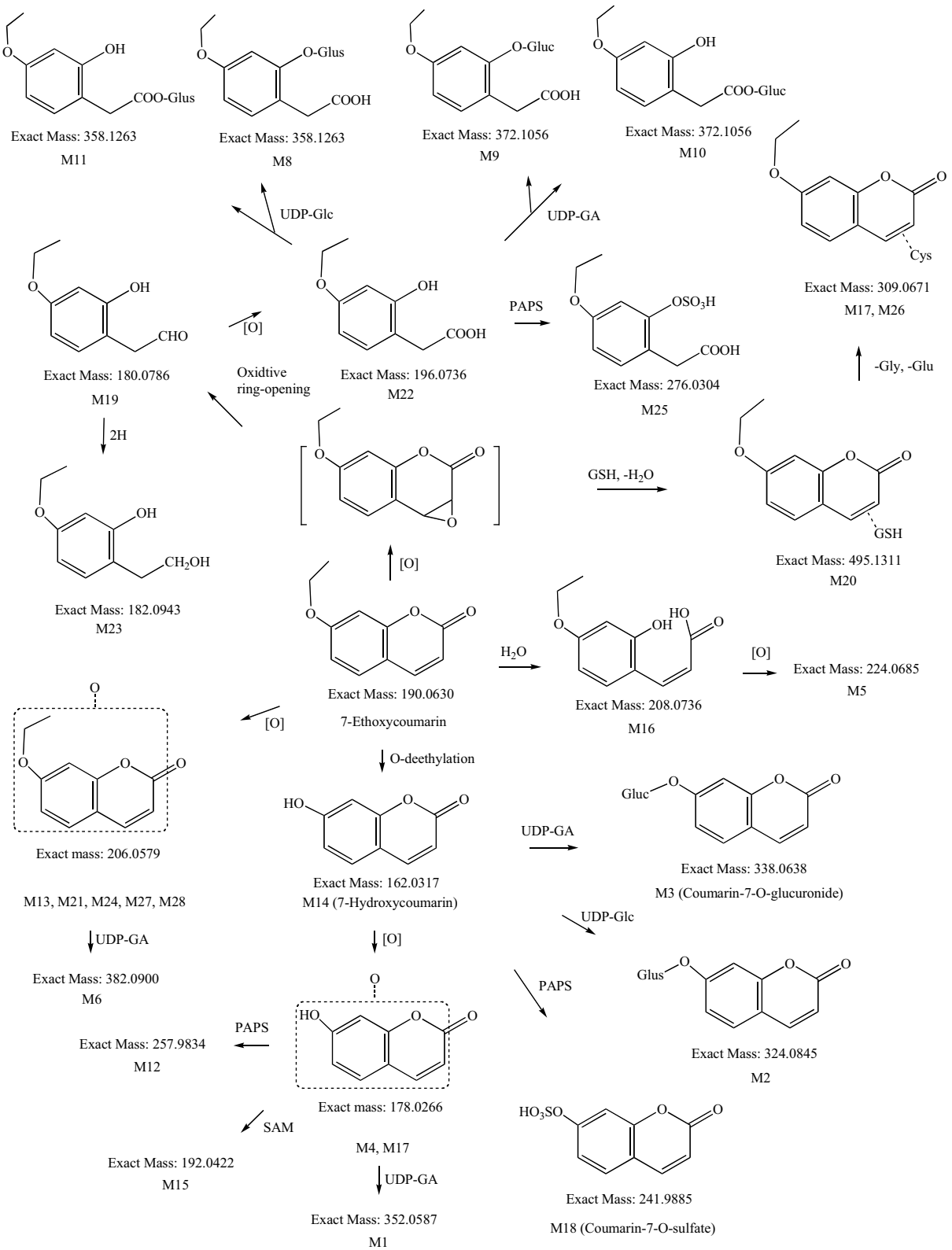

Scheme 10. Proposed metabolic pathways of 7-ethoxycoumarin in human and animal hepatocytes.

glutathionation. An epoxidation pathway was proposed to explain the formation of 2-hydroxy-7-ethoxyphenylacetaldehyde (M19), 2-hydroxy-7-ethoxyphenylethanol (M23), 2-hydroxy-7-ethoxyphenylacetic acid (M22), glucuronides (M9 and M10), and glucosides (M8 and M11). Glutathione conjugate (M20) and cysteine conjugates (M17, M26) were also generated from 7-ethoxycoumarin-3,4-epoxide *via* GSH addition and dehydrogenation, and glycine and glutamine hydrolysis, respectively. Chemical structures of metabolites and metabolic pathways are proposed in Scheme **10**. 7-Ethoxycoumarin 3, 4-peoxide was proposed as an interme-

diate. With an oxidative ring-opening pathway, overall metabolite contribution *via* this epoxidation pathway was estimated as 2.2% of 9.3% metabolites in human hepatocytes, 2.3% of 44.1% metabolites in monkey hepatocytes, 0.7% of 3.1% metabolites in dog hepatocytes, and 3.3% of 41.5% metabolites in rat hepatocytes. 7-Ethoxycoumarin 3,4-peoxide, M19 and M10 may be considered as reactive metabolites. An epoxide may bind enzymes and nucleic acids to cause cellular toxicity and genetic mutations, respectively. An acyl glucuronide (M10) may react with enzymes to form covalent drug-enzyme adducts *via* acyl migration or nucleophilic displacement to cause toxicity or immune hepatitis. An aldehyde (M19) as an electrophile may react with enzymes to form covalent drug-enzyme adducts to cause toxicity. Proposed 7-ethoxycoumarin 3,4-peoxide had the same *m/z* value as mono-oxygenated metabolites. It may not be stable enough to be detected, but was trapped as a glutathion conjugate (M20). The chemical structure of M19 was proposed as 4-ethoxy-2-hydroxylacetaldehyde. This structure was similar to 2-hydroxylacetaldehyde, a toxic metabolite of coumarin [1]. Although M19 only accounted for a very small portion (0.1 - 0.3%) of the total abundance and was only detected in negative ion mode across four species, and 7-ethoxycoumarin 3,4-peoxide may not be stable, it is still important to synthesize and confirm their chemical structures, and then evaluate their potential toxicity on humans and animals.

CONCLUSION

Following the incubation of 7-ethoxylcoumarin in male/female mixed human, male Cynomolgus monkey, male Beagle dog and male Sprague Dawley rat hepatocytes for 120 min, overall approximately 28 metabolites were detected and identified using high resolution liquid chromagraphy – tandem mass spectrometry in the positive ion and negative ion modes. O-deethylation, glucuronidation, sulfation, oxygenation, oxidative ring-opening, hydrogenation, glutathionation, dehydrogenation, cysteination, glucosidation, methylation, and hydrolysis were observed. At least sixteen metabolites not reported previously were newly identified, which were formed *via* additional oxidative ring-opening, hydrogenation, glutathionation, dehydrogenation, cysteination, glucosidation, methylation, and hydrolysis. M1, M3, M5, M14, M16, M22 and M27 exhibited high mass spectrometric responses in human hepatocytes. M3, M5, M8, M13, M14, M16, M18, M22 and M27 exhibited high mass spectrometric responses in monkey hepatocytes. M14, M16, M18, M20 and M27 exhibited high mass spectrometric responses in dog hepatocytes. M1, M3, M5, M13, M14, M16, M17, M18, M20, and M22 exhibited high mass spectrometric responses in rat hepatocytes. Species differences in metabolism of 7-ethoxylcoumarin in hepatocytes were observed across humans, monkeys, dogs and rats. The analysis of metabolites suggests that 7-ethoxylcoumarin may undergo 3,4-epoxidation responsible for formation of glutathione and its derived cysteine conjugates, carboxylic acid and its glucuronides, glucosides and sulfate, besides well-known 7-hydroxycoumarin, coumarin-7-O-glucuronide, and coumarin-7-O-glucuronide. The proposed chemical structures of 7-ethoxycoumarin 3,4-peoxide, M19 and M10 suggest that they may be reactive metabolites. It is important to confirm their structures by synthesizing metabolite standards and evaluate their potential toxicity.

ETHICS APPROVAL AND CONSENT TO PARTICIPATE

Not applicable.

HUMAN AND ANIMAL RIGHTS

No Animals/Humans were used for studies that are the basis of this research.

CONSENT FOR PUBLICATION

Not applicable.

CONFLICT OF INTEREST

The authors declare no conflict of interest, financial or otherwise.

ACKNOWLEDGEMENTS

The author(s) thank the reviewers' valuable comments and suggestion.

REFERENCES

[1] Chen, X.W.; Serag, E.S.; Sneed, K.B.; Zhou, S.F. Herbal bioactivation, molecular targets and the toxicity relevance, *Chem. Biol. Interact*., **2011**, *192(3)*, 161-76.

[2] Lake, B.G. Coumarin metabolism, toxicity and carcinogenicity: relevance for human risk assessment, *Food Chem. Toxicol*., **1999**, *37(4)*, 423-53.

[3] Vassallo, J.D.; Hicks, S.M.; Daston, G.P.; Lehman-McKeeman, L.D. Metabolic detoxification determines species differences in coumarin-induced hepatotoxicity, *Toxicol. Sci.* **2004**, *80(2)*, 249-57.

[4] Gerstel, D.; Jacques-Jamin, C.; Schepky, A.; Cubberley, R.; Eilstein, J.; Grégoire, S.; Hewitt, N.; Klaric, M.; Rothe, H.; Duplan, H. Comparison of protocols for measuring cosmetic ingredient distribution in human and pig skin, *Toxicol. In Vitro*., **2016**, *34*, 153-60.

[5] Riveiro, M.E.; De Kimpe, N.; Moglioni, A.; Vázquez, R.; Monczor, F.; Shayo, C.; Davio, C. Coumarins: old compounds with novel promising therapeutic perspectives. *Curr. Med. Chem*., **2010**, *17(13),* 1325-38.

[6] Wu, L.; Wang, X.; Xu, W.; Farzaneh, F.; Xu, R.The structure and pharmacological functions of coumarins and their derivatives, *Curr. Med. Chem*., **2009**, *16(32),* 4236-60.

[7] Yamazaki, H.; Inoue, K.; Mimura, M.; Oda, Y.; Guengerich F.P.; Shimada, T. 7-Ethoxycoumarin O-deethylation catalyzed by cytochromes P450 1A2 and 2E1 in human liver microsomes, *Biochem. Pharmacol*., **1996**, *51(3)*, 313-9.

[8] Shimada, T.; Tsumura, F.; Yamazaki, H. Prediction of human liver microsomal oxidations of 7-ethoxycoumarin and chlorzoxazone with kinetic parameters of recombinant cytochrome P-450 enzymes, *Drug Metab. Dispos.,* **1999**, *27(11)*, 1274-80.

[9] Uno, T.; Obe, Y.; Ogura, C.; Goto, T.; Yamamoto, K.; Nakamur, M.; Kanamaru, K.; Yamagata, H.; Imaishi, H. Metabolism of 7-ethoxycoumarin, safrole, flavanone and hydroxyflavanone by cytochrome P450 2A6 variants, *Biopharm. Drug. Dispos*., **2013**, *34(2)*, 87-97.

[10] Uno, T.; Nakano, R.; Kanamaru, K.; Takenaka, S.; Uno, Y.; Imaishi, H. Metabolism of 7-ethoxycoumarin, flavanone and steroids by

cytochrome P450 2C9 variants, *Biopharm. Drug Dispos*., **2017**, *38(8)*, 486-493.

[11] Woodhouse, K.W.; Mitchison, H.C.; Mutch, E.; Wright, P.D.; Rawlins, M.D.; James, O.F. The metabolism of 7-ethoxycoumarin in human liver microsomes and the effect of primary biliary cirrhosis: implications for studies of drug metabolism in liver disease, *Br. J. Clin. Pharmacol*., **1985,** *20(1)*, 77-80.

[12] Steensma, A.; Beamand, J.A.; Walters, D.G.; Price, R.J.; Lake, B.G. Metabolism of coumarin and 7-ethoxycoumarin by rat, mouse, guinea pig, cynomolgus monkey and human precision-cut liver slices, *Xenobiotica*, **1994**, *24(9)*, 893-907.

[13] Fisher, M.B.; Jackson, D.; Kaerner, A.; Wrighton, S.A.; Borel, A.G. Characterization by liquid chromatography-nuclear magnetic resonance spectroscopy and liquid chromatography-mass spectrometry of two coupled oxidative-conjugative metabolic pathways for 7-ethoxycoumarin in human liver microsomes treated with alamethicin, *Drug Metab. Dispos.,* **2002**, *30(3)*, 270-5.

[14] Uehara, S.; Uno, Y.; Oshio, T.; Inoue, T.; Sasaki, E.; Yamazaki, H. Marmoset pulmonary cytochrome P450 2F1 oxidizes biphenyl and 7-ethoxycoumarin and hepatic human P450 substrates, *Xenobiotica*, **2017**, *Jul 24*, 1-7, doi: 10.1080/00498254.2017.1354138 (Epub ahead of print)

[15] Terada, T.; Kaneko, H.; Terashita, S.; Tozuka, Z.; Tokuma, Y.; Hata, T. A species comparison of 14C-labeled 7-ethoxycoumarin metabolism in precision-cut liver slices from guinea pig and dog using a phosphor imaging system, *Res. Commun. Mol. Pathol. Pharmacol*., **1996**, *91(1)*, 41-56.

[16] Price, R.J.; Renwick, A.B.; Beamand, J.A.; Esclangon, F.; Wield, P.T.; Walters, D.G.; Lake, B.G. Comparison of the metabolism of 7-ethoxycoumarin and coumarin in precision-cut rat liver and lung slices, *Food Chem. Toxicol*., **1995**, *33(3)*, 233-7.

[17] Ball, S.E.; Thiel, V.E.; Tio, C.O.; Lim, H.K.; Kao, J.; Sisenwine, S.F.; Scatina, J. [14C]7-ethoxycoumarin metabolism by precision-cut rat hepatic slices, *Drug Metab. Dispos*., **1996**, *24(4)*, 383-9.

[18] Moloney, S.J.; Fromson, J.M.; Bridges, J.W. The metabolism of 7-ethoxycoumarin and 7-hydroxycoumarin by rat and hairless mouse skin strips, *Biochem. Pharmacol*., **1982**, *31(24)*, 4005-9.

[19] Albers, R.; Rosenberg, D.W. *In vivo* intestinal metabolism of 7-ethoxycoumarin in the rat: production and distribution of phase I and II metabolites in the isolated, perfused intestinal loop, *Toxicol. Appl. Pharmacol*., **1991**, *109(3)*, 507-13.

[20] Chikaoka, Y.; Tamura, M. 7-ethoxycoumarin deethylation activity in perfused isolated rat brain, *J. Biochem*., **1999**, *125(3)*, 634-40.

[21] Fry, J.R.; Bridges, J.W. The metabolism of 7-ethoxycoumarin in primary maintenance cultures of adult rat hepatocytes, *Naunyn Schmiedebergs Arch. Pharmacol*., **1980**, *311(1)*, 85-90.

[22] Gerson, R.J.; Serroni, A.; Gilfor, D.; Ellen, J.M.; Farber, J.L. Killing of cultured hepatocytes by the mixed-function oxidation of ethoxycoumarin, *Biochem. Pharmacol*., **1986**, *35(23)*, 4311-9.

[23] Kuki, W.; Hosotani, K.; Ohigashi, H.; Murakami, A. Metabolism and absorption of auraptene (7-geranyloxylcoumarin) in male SD rats: comparison with 7-ethoxycoumarin, *Nutr. Cancer*. **2008**, *60(3)*, 368-72.

[24] Jacques, C.; Perdu, E.; Dorio, C.; Bacqueville, D.; Mavon, A.; Zalko, D. Percutaneous absorption and metabolism of [14C]-ethoxycoumarin in a pig ear skin model, *Toxicol. In Vitro*., **2010**, *24(5)*, 1426-34.

[25] Aimoto, T.; Chiou, G.C. 7-ethoxycoumarin deethylase activity as indicator of oxidative metabolism in rabbit eyes, *J. Ocul. Pharmacol*., **1985**, *1(3)*, 279-86.

[26] Clement, B.; Mladek, C. Biotransformation processes in fertile hen's eggs. 1. Metabolic transformation of 7-ethoxycoumarin, *Pharmazie*, **1995**, *50(3)*, 207-10.

[27] Andersson, T.; Förlin, L.; Hansson, T. Biotransformation of 7-ethoxycoumarin in isolated perfused rainbow trout liver, *Drug Metab. Dispos*., **1983**, *11(5)*, 494-8.

[28] Sariaslani, F.S.; Rosazza, J.P. Novel Biotransformations of 7-Ethoxycoumarin by *Streptomyces griseus*, *Appl. Environ. Microbiol*., **1983**, *46(2)*, 468-74.

[29] Niraula, N.P.; Kanth, B.K.; Sohng, J.K.; Oh, T.J. Hydrogen peroxide-mediated dealkylation of 7-ethoxycoumarin by cytochrome P450 (CYP107AJ1) from *Streptomyces peucetius* ATCC27952, *Enzyme Microb. Technol*., **2011**, *48(2)*, 181-6.

[30] Uno, T.; Okamoto, S.; Masuda, S.; Itoh, A.; Uno, Y.; Nakamura, M.; Kanamaru, K.; Yamagata, H.; Imaishi, H. Bioconversion of small molecules by cytochrome P450 species expressed in *Escherichia coli*, *Biotechnol. Appl. Biochem*., **2008**, *50(Pt 4)*, 165-71.

[31] Kim, D.H.; Kim, K.H.; Kim, D.H.; Liu, K.H.; Jung, H.C.; Pan, J.G.; Yun, C.H. Generation of human metabolites of 7-ethoxycoumarin by bacterial cytochrome P450 BM3, *Drug Metab. Dispos*., **2008**, *36(11)*, 2166-70.

[32] Park, S.H.; Kim, D.H.; Kim, D.; Kim, D.H.; Jung, H.C.; Pan, J.G.; Ahn, T., Kim, D.; Yun, C.H. Engineering bacterial cytochrome P450 (P450) BM3 into a prototype with human P450 enzyme activity using indigo formation, *Drug Metab. Dispos*., **2010**, *38(5)*, 732-9.